Nuclear structure of ^{130}Te from inelastic neutron scattering and shell model analysis

S. F. Hicks,[1,2,*] A. E. Stuchbery,[3] T. H. Churchill,[4] D. Bandyopadhyay,[2] B. R. Champine,[4] B. J. Coombes,[3] C. M. Davoren,[1] J. C. Ellis,[1] W. M. Faulkner,[1] S. R. Lesher,[2,†] J. M. Mueller,[4] S. Mukhopadhyay,[2,‡] J. N. Orce,[2,§] M. D. Skubis,[4] J. R. Vanhoy,[4] and S. W. Yates[2,5]

[1]Department of Physics, University of Dallas, Irving, Texas 75062-4736, USA
[2]Department of Physics and Astronomy, University of Kentucky, Lexington, Kentucky 40506-0055, USA
[3]Department of Nuclear Physics, Research School of Physics, The Australian National University, Canberra ACT 2601, Australia
[4]Department of Physics, United States Naval Academy, Annapolis, Maryland 21402-5026, USA
[5]Department of Chemistry, University of Kentucky, Lexington, Kentucky 40506-0055, USA

(Received 6 June 2021; revised 13 September 2021; accepted 14 February 2022; published 28 February 2022)

Excited levels of ^{130}Te were studied with the $(n, n'\gamma)$ reaction. Excitation functions, $\gamma\gamma$ coincidences, angular distributions, and Doppler shifts were measured for γ rays from levels up to an excitation energy of 3.3 MeV. Detailed information that includes level lifetimes, multipole-mixing ratios, branching ratios, and electromagnetic transition rates deduced from these measurements is presented. Large-scale shell model calculations performed with all proton and neutron orbitals in the 50–82 shell are compared to these data, with generally good agreement, particularly for the positive-parity states. To investigate emerging collectivity in ^{130}Te, the Kumar-Cline sum rules were used to evaluate rotational invariants from the shell model calculations. Whereas the ground state and first-excited state show the greatest average deformation, as expected, all of the low-lying states are weakly deformed and triaxial.

DOI: 10.1103/PhysRevC.105.024329

I. INTRODUCTION

Historically, ^{130}Te was the first nucleus in which normal double-β decay ($\nu\nu\beta\beta$) was observed [1]. Its isotopic abundance of over 34%, the high $Q_{\beta\beta}$ value of 2527.518 $\pm$ 0.013 keV [2], and the ability to make very pure high-quality detectors from Te make it a leading candidate for observation of neutrinoless double-β decay ($0\nu\beta\beta$) as well [3]; CUORE and SNO+ are examples of large-scale $0\nu\beta\beta$ experimental collaborations using ^{130}Te as bolometric (TeO_2) [4] and scintillation (nat Te) detectors [5], respectively.

Extracting useful information regarding neutrino properties from a successful $0\nu\beta\beta$ half-life measurement will require detailed knowledge of the nuclear matrix element (NME) linking the ground states of the parent and daughter nuclei, which in this case are ^{130}Te and ^{130}Xe, respectively; this matrix element must be calculated by nuclear structure theory, and current models predict values differing by nearly a factor of three for $A = 130$ [6].

In addition to its importance to $0\nu\beta\beta$ investigations, ^{130}Te is the heaviest stable isotope of an isotopic chain that offers six stable even-mass nuclei with $Z = 52$ for studying the evolution of structure from near the $N = 82$ neutron shell closure to ^{120}Te, near midshell at $N = 66$. The monotonic increase of $B(E2; 2_1^+ \rightarrow 0_1^+)$ values from $N = 82$ to midshell reflect a growth of collectivity across the isotopic chain, and the ratio of the 4_1^+ to 2_1^+ level energy ($R_{4/2}$) has a range of $1.95 \leqslant R_{4/2} \leqslant 2.09$, as expected for vibrational nuclei [7].

The systematic behavior of level energies across the isotopic chain shown in Fig. 1 indicates a simple vibrational picture is woefully incomplete for the Te nuclei. The near constancy of the 6_1^+ level energy across the stable isotopes is not typical of a three-quadrupole-phonon vibrational state, and the "V"-shaped behavior of the energies of the 0_2^+ and 0_3^+ states may be evidence of shape coexistence [8–10]. While the particlelike nature of the former for ^{130}Te has long-been established [11,12] and recently confirmed in shell model calculations [13–17], the lack of experimental level information, especially the characteristics of excited 0^+ states, in ^{130}Te has limited investigations of shape coexistence in this nucleus; only the 0_2^+ state has previously been identified [18].

Sharma, Devi and Khosa [19] studied shape changes across the tellurium isotopic chain based on relativistic Hartree-Bogoliubov calculations with two alternative effective interactions. Their work suggests that ^{130}Te is spherical or very near spherical, which supports the application of the shell model.

Recently, considerable effort has been invested in large-scale shell-model calculations to investigate various aspects of the structure of nuclei in this mass region. A comprehensive study of $A = 130$ nuclei was completed by Teruga *et al.*

*hicks@udallas.edu
†Present Address: Department of Physics, University of Wisconsin-La Crosse, La Crosse, Wisconsin 54601-3742, USA.
‡Present Address: Department of Nuclear and Radiological Engineering and Medical Physics, Georgia Institute of Technology, Atlanta, Georgia 30332-0745, USA.
§Present Address: Department of Physics, University of the Western Cape, P/B X17, Bellville ZA-7535, South Africa.

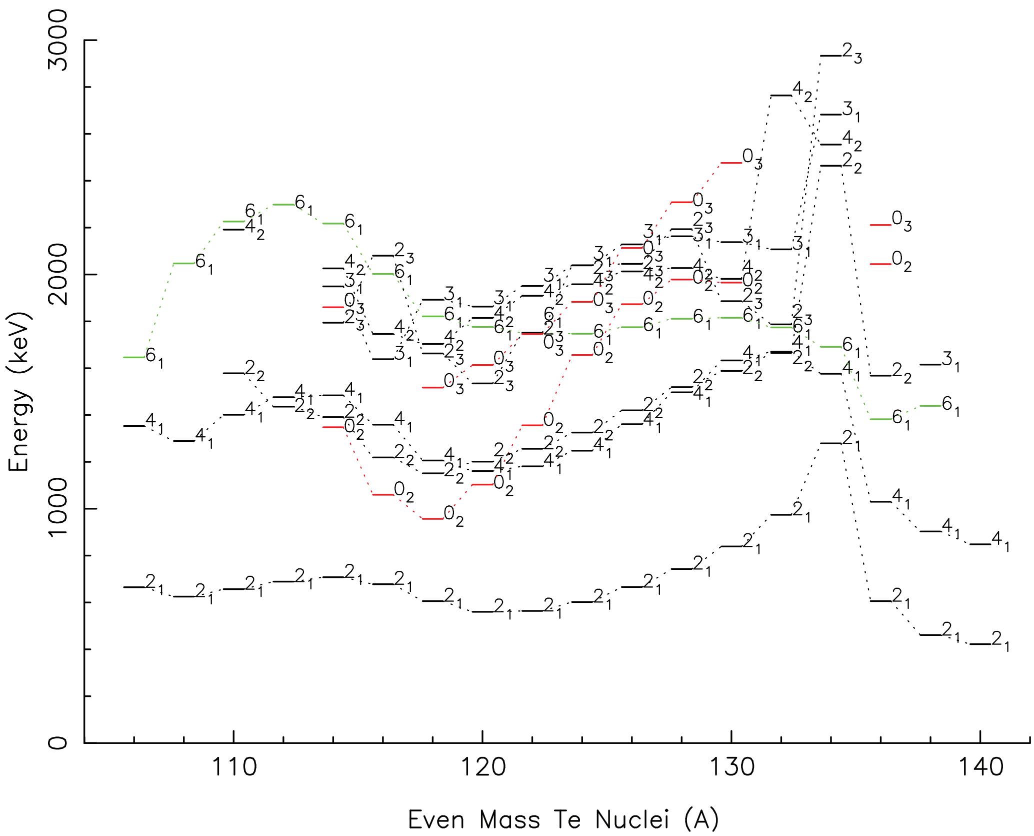

FIG. 1. Energies of low-lying positive-parity states across the Te isotopic chain from Ref. [7] and the present $(n,\, n'\gamma)$ results for ^{130}Te. Included are states that have long been considered members of the 1-, 2-, and 3-quadrupole phonon multiplets in a vibrational picture. Clear deviations of expected systematic behavior for collective vibrations are shown for the lowest two 0^+ levels, highlighted in red, and for the 6_1^+ levels, highlighted in green.

[14], of neutron-core excitations and low-lying state properties of $^{130-134}$Te by Wang *et al.* [16], emerging collectivity in the stable Te isotopes by Coombes *et al.* [17], magnetic moments by Jakob *et al.* [20], Stuchbery *et al.* [21] and Brown *et al.* [22], and NMEs for $0\nu\beta\beta$ studies by Neacsu and Horoi [13]. Qi [23] calculated the yrast states up to 12^+ and $B(E2;2_1^+ \rightarrow 0_1^+)$ values for the Te isotopes from $N = 52$ to $N = 82$. Bianco *et al.* [24] performed shell model calculations of the electromagnetic transitions from the low-lying 2^+ states to investigate proton-neutron correlations and the concept of mixed-symmetry states. Lei, Zhao, and Arima used ^{130}Te, along with neighboring ^{131}Te and ^{132}I, to study the validity of the nucleon pair approximation as a means to truncate shell model calculations [25].

The model space used in these works invariably included the $0g_{7/2}$, $1d_{5/2}$, $1d_{3/2}$, $2s_{1/2}$, and $0h_{11/2}$ single-particle orbitals for neutrons and protons separately, while Wang *et al.* [16] included the $1f_{7/2}$ and $2p_{3/2}$ orbitals above $N = 82$ to study neutron core excitations and evaluate $E1$ transitions. These previous studies differed by the interactions used in the calculations; however, all were limited by a lack of empirical evidence for testing the validity of their results.

Existing information on the adopted levels of ^{130}Te [18] is derived from reactor (n, n$'\gamma$) [26], (n, n$'\gamma$) with accelerator-produced neutrons [27], β^- decay [28,29], $\beta\gamma$ coincidence [30], (γ, γ') [31,32], ^{130}Te(^{64}Ni, Xγ) [33], Coulomb excitation [17,21,34,35], g-factor [17,36,37], and scattering [38–45] measurements. Absent from these measurements is extensive transition-rate data and detailed level information required for model validation, which is necessary for deducing neutrino properties from $0\nu\beta\beta$ measurements and for our understanding of nuclear structure in the $Z = 52$ isotopes.

To provide this needed experimental information, the results from a series of $(n,\, n'\gamma)$ measurements on ^{130}Te are reported. New large-basis shell model calculations are also presented, along with a comparison of these model calculations with new experimental results to investigate the role of collective and few-particle excitations in ^{130}Te.

II. EXPERIMENTAL METHODS

Measurements were performed using the 7 MV CN Van de Graaff accelerator and the neutron production and γ-ray detection facilities at the University of Kentucky Accelerator Laboratory (UKAL). The proton beam was terminally pulsed and then bunched resulting in a time spread of $\Delta t \approx 1$ ns. The ^{3}H$(p,n)^3$He reaction was used as a neutron source with ^{3}H gas pressures of $\approx$0.9 atm used for all measurements. For the ^{130}Te measurements with a singles γ-ray detector configuration, a 48.6641 g metallic five-piece sample, isotopically enriched to 99.47(1)%, was tightly wrapped with plastic to

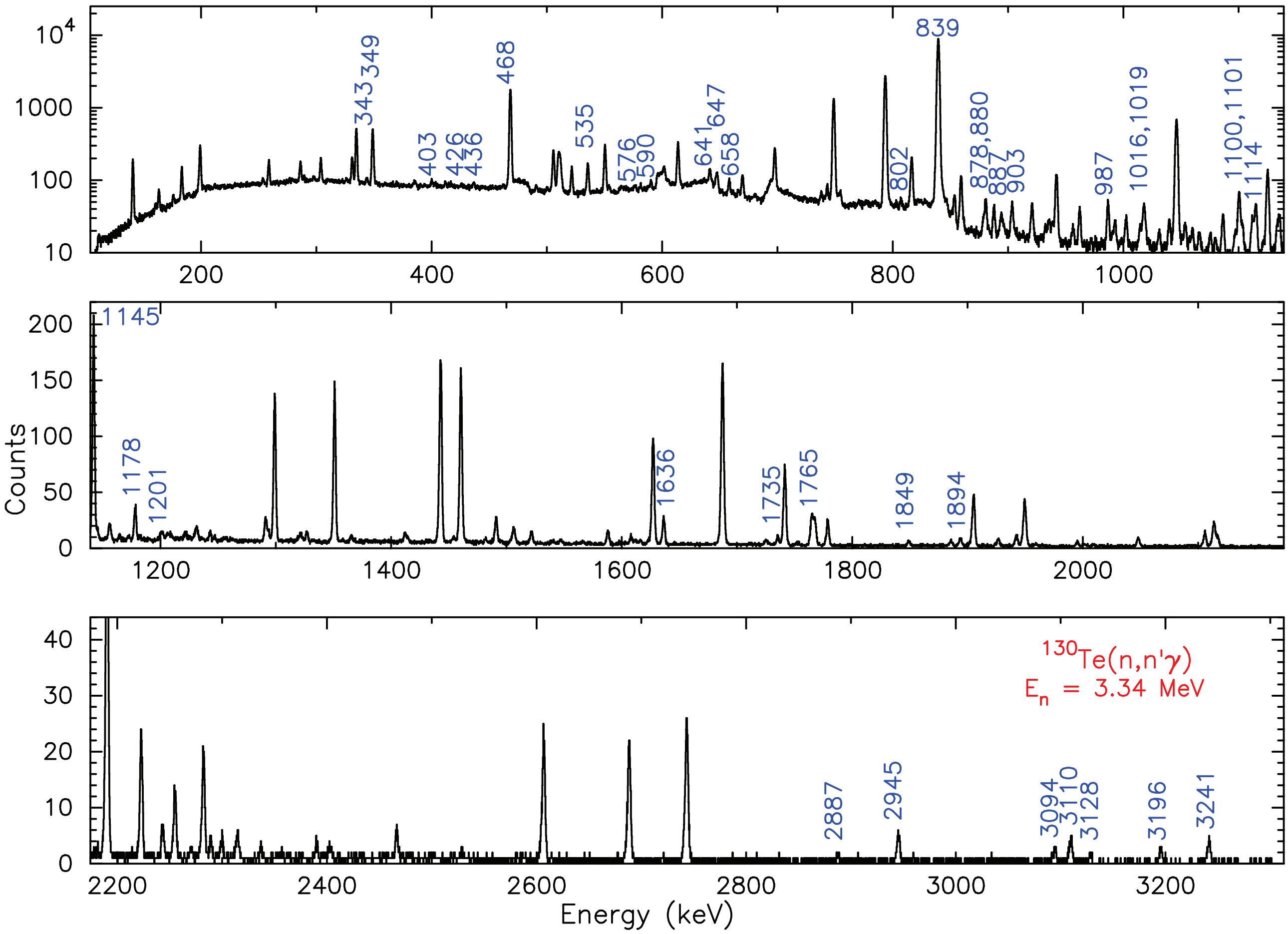

FIG. 2. Singles γ-ray spectrum from the ^{130}Te $(n, n'\gamma)$ reaction at $E_n = 3.34$ MeV shown in panels (a) through (c). Newly placed γ rays from levels below 2.8 MeV excitation and new ground-state transitions are denoted by energy (blue).

approximately cylindrical shape with a diameter of 2.05 cm and height of 3.80 cm. The sample used for the $\gamma\gamma$ coincidence measurements was $\approx$100 g of natural tellurium chips placed in a thin-walled polyethylene container.

γ-ray excitation functions, angular distributions, and Doppler shifts were measured with a singles γ-ray detector configuration. For this arrangement, a Compton-suppressed n-type HPGe detector with 53% relative efficiency and an energy resolution of $\approx$2.1 keV FWHM at 1.33 MeV was used. A bismuth germanate (BGO) annular detector surrounding the main detector was used for Compton suppression and as an active shield. The gain stability of the system was monitored using a radioactive ^{226}Ra source, which was also used for energy and efficiency calibrations of the main detector. All radioactive source measurements were performed without beam on target for short durations between detector angle changes to monitor possible shifts and for long durations both before and after experimental runs for calibrations. The neutron scattering facilities, TOF neutron background suppression, neutron monitoring and data reduction techniques have been described elsewhere [46]. A spectrum from the γ-ray excitation function measurements at an incident neutron energy of $E_n = 3.34$ MeV is shown in Fig. 2.

γ-ray excitation functions measured at incident neutron energies between 1.86 and 3.34 MeV in 90 keV steps were used to place γ rays in the level scheme, to assist in spin assignments, and to determine branching ratios. Theoretical neutron scattering cross sections and γ-ray production yields were calculated using the statistical model code CINDY [47] with optical model parameters appropriate for this mass and energy region [48]. Experimental γ-ray production cross sections were then compared to theoretical values for each level to assess level spins and γ-ray branching ratios. The center-of-gas-cell to center-of-sample distance was 6.3(1) cm, and the flight path from the sample center to the detector face was 112(1) cm for the excitation function measurements. Sample experimental and model excitation functions are shown in Fig. 3 and discussed below in more detail.

For $\gamma\gamma$ coincidence measurements, 3.5 MeV neutrons emerging from the source reaction were formed into a 1 cm beam by the use of a lithium-loaded collimator approximately 75 cm long. The natural tellurium sample was hung coaxially with this beam, and four high-efficiency HPGe detectors were placed in a transverse arrangement between 4.1 cm and 5.5 cm from the sample. The singles rates were about 3K on each detector, while the coincidence rate was approximately 400/s.

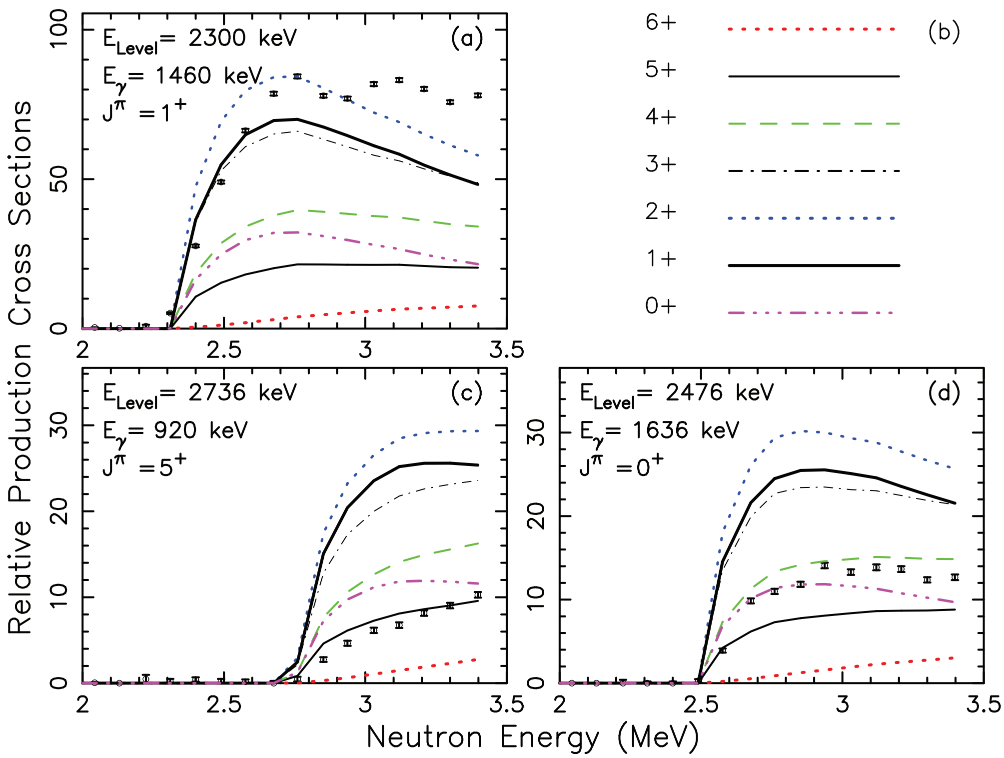

FIG. 3. Relative γ-ray production cross sections observed in ^{130}Te compared to statistical model calculations (SMC) for the 1460, 920, and 1636 keV γ rays in panels (a), (c), and (d), respectively, while the legend is shown in panel (b). The good agreement between calculations and data support both the γ-ray branching ratios and spin assignments of the levels shown. The effect of feeding from higher-lying levels can be seen in both panels (a) and (d) at about 2.9 MeV.

Data were stored in event mode, and a two-dimensional matrix was constructed off line by considering pairwise coincidences.

Examples of the use of γ-ray excitation functions in combination with $\gamma\gamma$ coincidence data are shown in Fig. 4. A portion of Gate(1046) [where Gate(1046) denotes a coincidence gate on the 1046.2 keV γ ray produced in the $^{\mathrm{nat}}$Te(n, n$'\gamma\gamma$) reaction] from the $2_3^+ \rightarrow 2_1^+$ transition in ^{130}Te is shown in the top panel of Fig. 4, along with the excitation functions of the 881 and 903 keV (doublet) γ rays, and the bottom panel shows a section of Gate(468) from the $5_1^- \rightarrow 6_1^+$ transition, along with the excitation function of the 1086 keV γ ray. Combining excitation function singles and coincidence data offers a powerful method for building the level scheme of a nucleus.

Angular distributions of γ rays were measured at neutron energies of 2.2 and 3.3 MeV. For the angular distributions the sample center was located 8.5(1) cm from the center of the gas cell, while the detector face was 115(1) cm from the center of pivot, which was also the sample center. These angular distributions were fit to even-order Legendre polynomial expansions and compared to calculations from the statistical model code CINDY [47] to extract level spins and multipole-mixing ratios. The angular distribution of the 1103 keV γ ray and its corresponding χ^2 versus $\tan^{-1}(\delta)$ plot are shown in Figs. 5(a) and 5(b), while the angular distributions of the 1145 and 1894 keV γ rays are shown in Figs. 5(c) and 5(d).

Level lifetimes were extracted using the Doppler-shift attenuation method following inelastic neutron scattering (INS). Angular distributions measured at the E_n closer to the level threshold were used to find Doppler shifts from γ-ray centroids to avoid complications from feeding. For the recoil energies present in this experiment, the γ-ray centroids have the following angular dependence:

$$E_\gamma(\theta) = E_0\,[1 + F_{\mathrm{exp}}\beta\ \cos(\theta)], \tag{1}$$

where E_0 is the unshifted γ-ray energy, F_{exp} is the Doppler-shift attenuation factor which carries the dependence on lifetime, $\beta = v_{\mathrm{cm}}/c$, θ is the γ-ray emission angle with respect to the incident neutron beam, and $E_\gamma(\theta)$ is the γ-ray energy measured at the angle θ. Lifetimes were determined by comparing F_{exp} with calculated values using the stopping theory of Winterbon [49]. This method has been shown to yield reliable lifetimes with a variety of targets with mean lifetimes in the range of ~2 fs to ~2 ps as deduced in these measurements [50,51]. Doppler shifts for the 2282-, 1765-, and 2689-keV γ rays, as well as the theoretical curve used to extract the mean lifetime τ, are shown in Fig. 6.

III. EXPERIMENTAL RESULTS

The techniques outlined above were used to place γ rays in a level scheme extending to 3.3 MeV excitation energy. Level energies, spin and parity assignments, γ-ray decays, γ-ray branching ratios, multipole-mixing ratios, Doppler-shift attenuation factors, mean lifetimes, and transition rates for all observed levels are given in Table I. The legend description

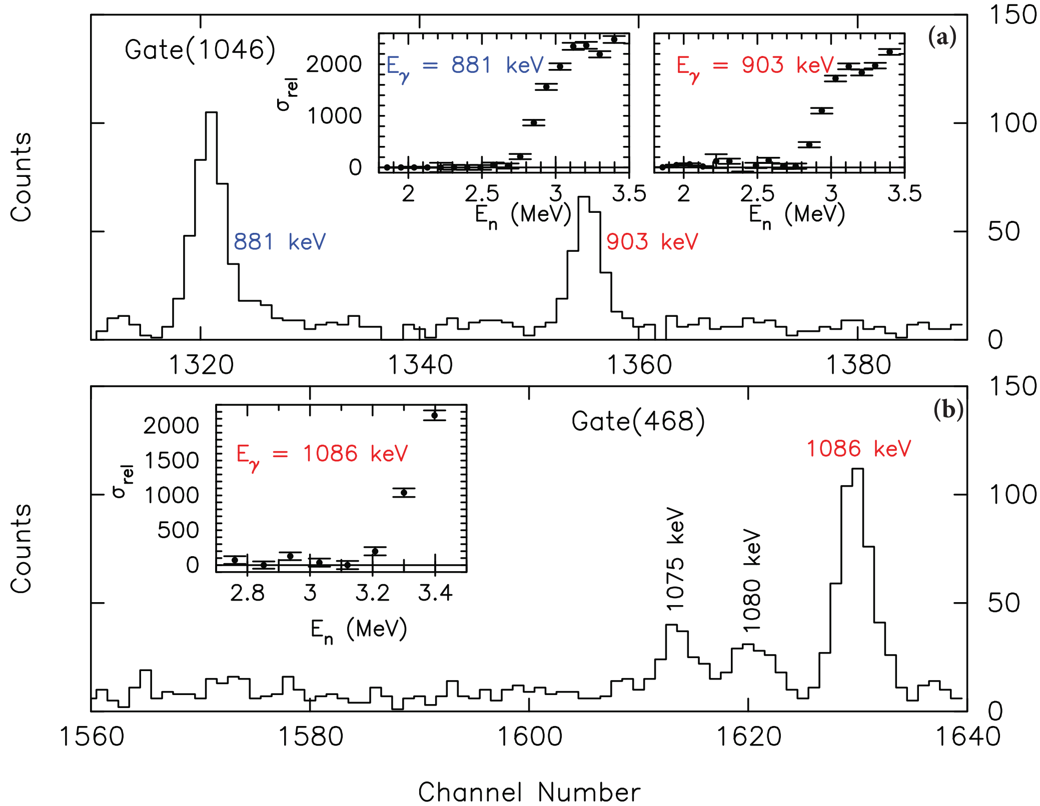

FIG. 4. A portion of the γ-ray coincidence spectrum from a gate on the $2_3^+ \rightarrow 2_1^+$ transition, Gate(1046), in panel (a), along with excitation functions of the 881 and 903 keV (doublet) γ rays; a portion of the spectrum from a gate on the $5_1^- \rightarrow 6_1^+$ transition, Gate(468), along with the excitation function of the 1086 keV γ ray in panel (b). The γ rays labeled in the figures belong to newly identified levels or indicate possible spurious assignments in ^{130}Te [18].

for the *Notes* column is at the end of Table I. Only states with observed differences from the adopted level scheme for ^{130}Te [18] are examined in detail in Sec. II A. Comparisons with previous experimental results are provided in Sec. II B. Legendre polynomial coefficients for γ rays placed in this work can be found in Table VIII in the Appendix.

A. Level discussion

States with angular momentum above J = 6 are typically not observed in $(n, n'\gamma)$ measurements at UKAL unless they are fed significantly from higher-lying excited levels. Missing adopted states with known J $\geqslant$ 7 are not discussed below.

1. Possible spurious adopted levels

(2719 keV 5^+ *level).* This level is adopted [18] with 738.1, 904.0, and 1086.5 keV γ rays from reactor $(n, n'\gamma)$ experiments [26]. In this new INS study, the 903.4 keV γ ray is assigned to the 2789.1 keV level from its excitation function and presence in Gate(1046), as shown in the top panel of Fig. 4, while the unresolved 905.1 keV γ is assigned to the 3006.4 keV level based on its presence in Gate(468) (although not shown in Fig. 4), Gate(793) and Gate(839), as well as the second threshold observed in its excitation function. The 1086-keV γ ray is observed in the same gates and has a threshold >3.0 MeV, as shown in the bottom panel of Fig. 4, and is assigned to a new level at 3187.7 keV. The 738-keV γ ray has a strong background component in this work and cannot be eliminated completely, but it is not observed in Gate(348). This level appears to be spurious.

(2729.5 keV 3^- *level).* This level is adopted [18] with a single tentatively placed 1890 keV γ ray [26]. The level has also been reported from multiple inelastic scattering experiments [18], some with large energy uncertainties. No evidence of an 1890 keV or other γ ray belonging to this level was observed in this work, which may mean its intensity is below our detection threshold; however, states with $J^\pi = 3^-$ are typically populated in $(n, n'\gamma)$ experiments and usually γ rays are observed from $E1$ decays to lower-lying positive-parity levels.

2. Adopted levels with new information

2146.0 keV 7^- *level.* The adopted 330.7 keV γ ray from this level to the 6_1^+ state [18] is observed and supported in the coincidence gates. Its angular distribution supports J = 7 or J = 5, with no multipole mixing for the former, i.e., it represents a pure dipole transition. Further analysis is complicated by the unresolved 331.1 keV γ ray assigned to the 2432.3 keV level. The tentatively adopted 46 keV γ ray from the 2146.0 keV state is below the detection threshold in this work, but the immediate departure of the 5_1^- excitation function away from SMC described above supports the assignment indirectly, as it indicates the rapid onset of feeding. Comparison

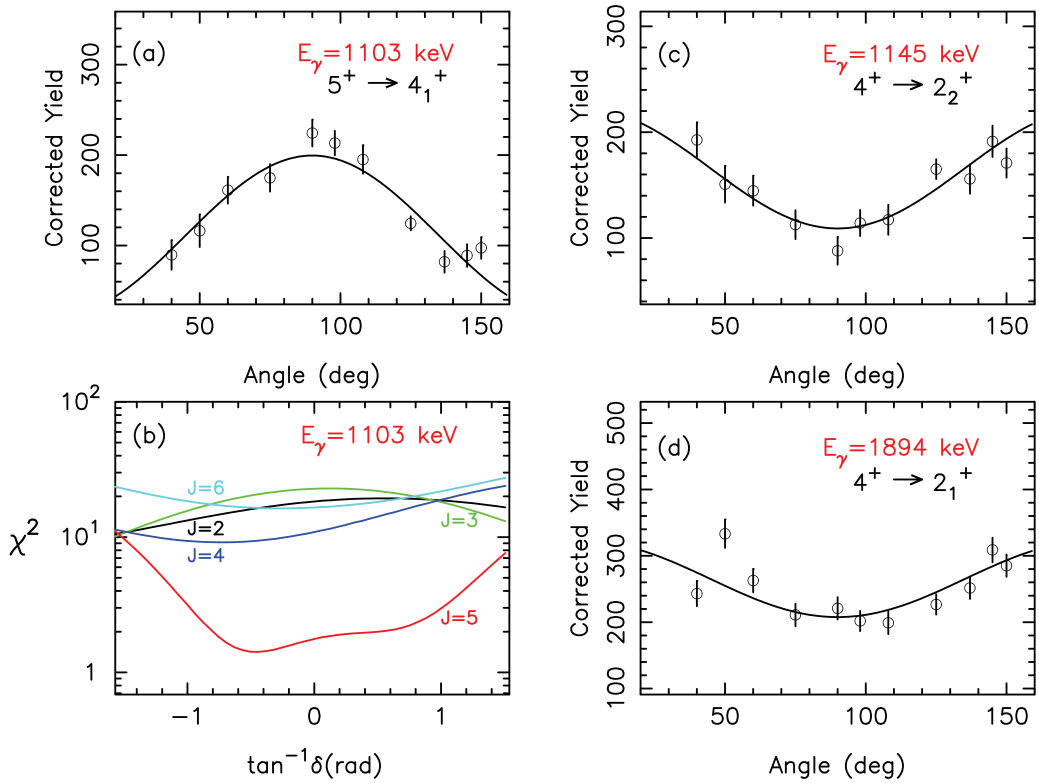

FIG. 5. Angular distributions for the 1103, 1145, and 1894 keV γ rays in panels (a), (c), and (d), respectively. The χ^2 versus $\tan^{-1}(\delta)$ plots used to deduce the $E2/M1$ multipole-mixing ratio for the 1103 keV γ ray is shown in panel (b) with each curve labeled by the spin of the final state: J = 2 (black), J = 3 (green), J = 4 (blue), and J = 6 (aqua). The spin of the 2736 keV level is deduced from panels (a) and (b) as J = 5, and the spin of the 2733 keV level is determined to be J = 4 from panels (c) and (d), while $J^\pi = 3^-$ is eliminated as a possible spin for either level. All shown angular distributions were measured at $E_n = 3.3$ MeV.

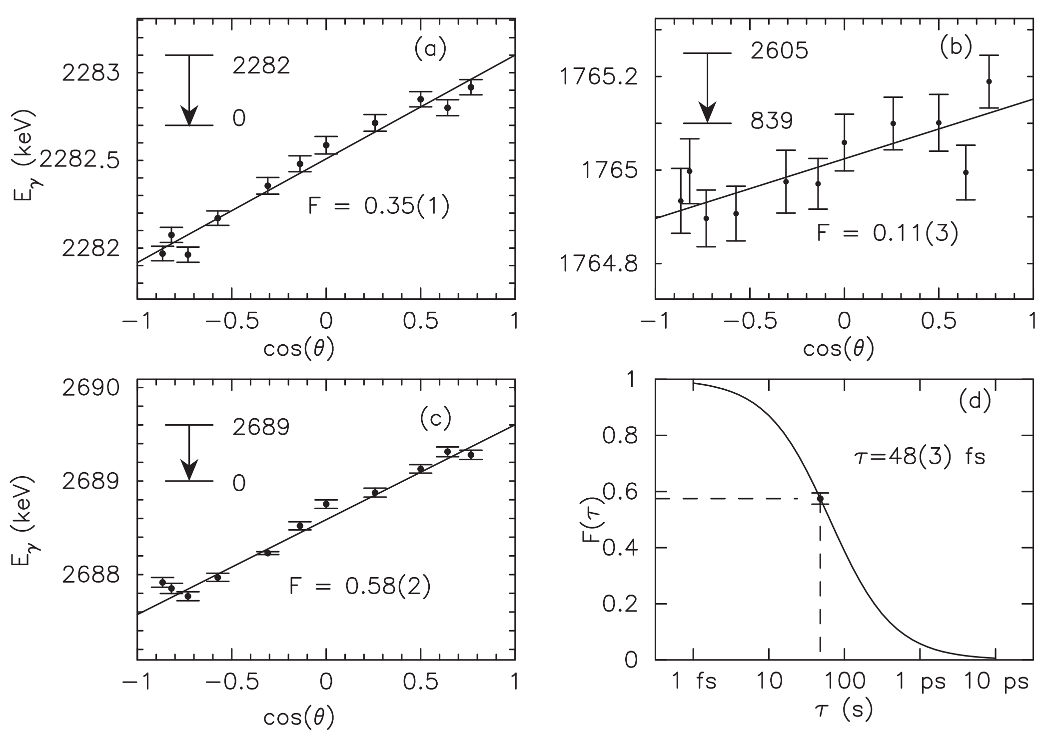

FIG. 6. Doppler shifts for the (a) 2282, (b) 1765, and (c) 2689 keV γ rays in ^{130}Te. The stopping theory calculation used to deduce the mean lifetime, τ, from the Doppler shift of the 2689 keV γ ray is shown in panel (d).

TABLE I. Levels in ^{130}Te. Uncertainties are in the last digit(s). Multipole-mixing ratios which could not be determined are denoted by "—," where upper limits are given for the respective transition strengths when the lifetime of the level is known. This limit often leads to reduced transition probabilities that are unreasonably large. The attenuation factor $\bar{F}$ is the average value for the level. Levels below 2.2 MeV in excitation were evaluated using the angular distribution data at $E_n = 2.2$ MeV unless otherwise noted. The following Weisskopf units are used: B($E1$), 1 e^{2}fm^2 = 1.65 W.u.; B($E2$), 1 e^{2}fm^4 = 39.1 W.u.; and B($M1$), 1 μ_{N^2} = 1.79 W.u. for ^{130}Te. B($E1$) values are in W.u. Transition rate uncertainties were determined using TRANSNUCLEAR (unpublished), which determines the overall uncertainty from the limits of the γ-ray energies, branching ratios, multipole-mixing ratios, and level lifetimes.

J^π	Note	E_x (keV)	E_γ (keV)	E_f (keV)	BR %	XL/δ[a]	$\bar{F}$	τ (fs)	B(M1) (μ_N^2)	B(E2) (W.u.)
2^+		839.49(5)	839.49(5)	0	100	E2		3320(70)[b]		15.1(3)[b],[c]
2^+		1588.19(5)	748.73(6)	839	98.12(3)	0.63^{+27}_{-23}	<0.042	>1310	$<4.0 \times 10^{-2}$	<19
			1588.14(6)	0	1.88(3)	E2				<0.030
4^+		1632.97(8)	793.48(6)	839	100	E2				14(3)[f]
6^+		1815.37(21)	182.39(20)	1632	100	E2		14.1(7)ns[b]		6.1(3)[b]
2^+		1885.66(6)	1046.15(5)	839	98.47(4)	3.9^{+10}_{-5}	0.120(9)	430^{+40}_{-40}	$7.0^{+20}_{-28} \times 10^{-3}$	36^{+17}_{-9}
						-0.19^{+11}_{-4}			$1.1^{+2}_{-2} \times 10^{-1}$	1.3^{+2}_{-2}
			1885.70(9)	0	1.53(4)	E2				0.031^{+5}_{-4}
0^+		1964.69(6)	1125.20(5)	839	100	E2	0.023(11)	2600^{+2400}_{-900}[h]		4.4^{+22}_{-22}
4^+	d	1981.43(11)	348.5(2)	1632	53.4(3)	0.22^{+48}_{-17}	0.020(7)	2800^{+1500}_{-800}[h]	$2.4^{+11}_{-11} \times 10^{-1}$	35^{+20}_{-14}
			1141.93(5)	839	46.6(3)	E2				1.8^{+7}_{-7}
5^-		2101.27(6)	468.3(2)	1632	100	E1				
3^+		2138.55(5)	505.62(6)	1632	18(1)	1.1^{+8}_{-8}	0.014(8)	4400^{+5500}_{-1600}	$8.0^{+110}_{-63} \times 10^{-3}$	15^{+21}_{-12}
			550.30(6)	1588	41(1)	1.3^{+6}_{-6}			$1.2^{+15}_{-9} \times 10^{-2}$	24^{+28}_{-18}
			1299.07(5)	839	41(1)	0.51^{+21}_{-17}			$1.9^{+15}_{-12} \times 10^{-3}$	0.11^{+9}_{-7}
7^-	xd	2146.04(29)	330.67(21)	1815	100	E1		166^{+12}_{-12}ns[b]	B(E1)=$6.4^{+5}_{-5} \times 10^{-8}$	
2^+		2190.49(7)	1351.01(5)	839	40(1)	-2.0^{+28}_{-17}[e]	0.096(6)	590^{+40}_{-40}	$3.2^{+58}_{-31} \times 10^{-3}$	2.5^{+28}_{-25}
			2190.45(10)	0	60(1)	E2				0.42^{+4}_{-4}
2^+	f	2282.51(7)	1443.02(5)	839	84(1)	3.9^{+15}_{-15}	0.352(6)	120^{+10}_{-10}	$8.4^{+45}_{-43} \times 10^{-3}$	23^{+13}_{-12}
						-0.16^{+11}_{-11}			$1.3^{+7}_{-7} \times 10^{-1}$	0.60^{+4}_{-4}
			2282.51(10)	0	16(1)	E2				0.46^{+5}_{-4}
$(1^+, 2^+)$	xd	2300.11(7)	1460.62(5)	839	96(1)	-0.78^{+85}_{-76}	0.085(8)	670^{+80}_{-70}	$1.6^{+12}_{-9} \times 10^{-2}$	1.7^{+12}_{-17}
			2300.16(12)	0	4(1)	M1			$2.8^{+11}_{-9} \times 10^{-4}$	
4^+	xdgn	2330.66(9)	349.35(22)	1981	13(2)	—[i]	0.067(12)	860^{+200}_{-140}	⩽0.24	⩽820[i]
			697.68(5)	1632	70(5)	-0.03^{+9}_{-3}			$1.3^{+4}_{-4} \times 10^{-1}$	0.092^{+26}_{-92}
						1.0^{+2}_{-2}			$6.7^{+26}_{-22} \times 10^{-2}$	51^{+20}_{-17}
			1491.17(6)	839	17(3)	E2				0.56^{+23}_{-19}
6^-	xm	2405.0(2)	258.83(20)	2146	49(1)	5.2^{+17}_{-9}				

TABLE I. (Continued.)

J^π	Note	E_x (keV)	E_γ (keV)	E_f (keV)	BR %	XL/δ[a]	$\bar{F}$	τ (fs)	B(M1) (μ_N^2)	B(E2) (W.u.)
						0.25^{+7}_{-5}				
			303.87(20)	2101	51(1)	0.03^{+3}_{-3}				
	x	2432.3(2)	286.23(20)	2146	[26(3)][b]					
$(6^+, 7^-)$										
	d		331.1(5)	2101	[74(3)][b]					
4^-		2435.96(5)	334.69(20)	2101	100	-0.06^{+6}_{-3}				
4^+	xdn	2449.41(7)	467.90(23)	1981	20(4)	–[j]	0.141(13)	380^{+50}_{-40}	$\leqslant 0.39$	$\leqslant 650$[j]
			816.42(5)	1632	80(4)	-0.22^{+10}_{-8}			0.21^{+4}_{-4}	5.6^{+10}_{-9}
						1.5^{+3}_{-2}			$6.7^{+18}_{-20} \times 10^{-2}$	84^{+28}_{-20}
2^+	xmn	2466.85(5)	581.10(7)	1885	4.6(3)	-0.32^{+45}_{-56}	0.070(9)	820^{+130}_{-100}	0.015^{+5}_{-6}	1.6^{+8}_{-16}
						5.2^{+540}_{-98}				
	n		878.73(8)	1588	4.3(3)	-0.26^{+33}_{-37}			$4.1^{+12}_{-11} \times 10^{-3}$	0.13^{+5}_{-13}
						5.2^{+110}_{-78}				
			1627.37(5)	839	80.1(4)	-16^{+25}_{-28}			$4.7^{+120}_{-47} \times 10^{-5}$	1.8^{+50}_{-18}
						-0.51^{+12}_{-12}			0.010^{+3}_{-3}	0.37^{+8}_{-8}
			2466.91(11)	0	11.0(2)	E2				0.031^{+5}_{-5}
0^+	ln	2476.00(5)	590.36(6)	1885	20.1(10)	E2	0.034(22)	1800^{+2600}_{-700}		33^{+24}_{-21}
	n		887.81(6)	1588	28.8(6)	E2				6.2^{+42}_{-38}
	n		1636.49(6)	839	51.1(7)	E2				0.52^{+34}_{-32}
3^-	xfn	2527.11(14)	425.86(22)	2101	0.8(3)	E2				
	n		641.44(6)	1885	8.7(20)	E1				
			894.10(6)	1632	3.1(5)	E1				
	n		939.1(5)	1588	0.9(3)	E1				
			1687.63(5)	839	86.5(20)	E1				
$(7^-,6)$	ln	2537.48(22)	436.48(21)	2101	100					
3^+	x	2575.00(5)	942.01(5)	1632	68.0(3)	0.03^{+10}_{-6}	0.077(14)	740^{+180}_{-130}	$6.2^{+14}_{-13} \times 10^{-2}$	$2.3^{+5}_{-23} \times 10^{-2}$
	n		986.74(6)	1588	24.1(3)	-16^{+17}_{-9}			$7^{+15}_{-6} \times 10^{-5}$	7.2^{+84}_{-72}
						0.13^{+10}_{-4}			$1.9^{+5}_{-4} \times 10^{-2}$	0.12^{+3}_{-3}
	n		1735.67(7)	839	7.9(3)	-0.19^{+11}_{-13}			$1.1^{+3}_{-3} \times 10^{-3}$	$4.9^{+13}_{-12} \times 10^{-3}$
						-2.5^{+12}_{-7}			$1.6^{+10}_{-11} \times 10^{-4}$	0.12^{+12}_{-6}
2^+	x	2581.00(6)	992.77(6)	1588	10.2(3)	1.7^{+8}_{-14}	0.174(9)	300^{+20}_{-20}	$5.1^{+51}_{-27} \times 10^{-3}$	5.5^{+32}_{-48}
						0.16^{+35}_{-20}			$1.9^{+3}_{-3} \times 10^{-2}$	0.19^{+3}_{-19}
			1741.53(5)	839	89.8(3)	0.68^{+24}_{-28}			$2.2^{+6}_{-5} \times 10^{-2}$	1.3^{+3}_{-3}
(0^+)	dlfgmn	2604.52(8)	1016.3(8)	1588	8(6)	E2	0.110(30)	500^{+190}_{-110}		3.1^{+39}_{-26}
	fmn		1765.02(6)	839	92(6)	E2				2.3^{+9}_{-8}
$1^{(+)}$	xfn	2607.2(2)	1019.2(5)	1588	6(5)	–	0.383(13)	100^{+10}_{-10}	$\leqslant 0.061$	$\leqslant 22$
	f		1767.77(6)	839	31(6)	–			$\leqslant 0.040$	$\leqslant 4.7$

TABLE I. (*Continued.*)

J^π	Note	E_x (keV)	E_γ (keV)	E_f (keV)	BR %	XL/δ[a]	$\bar{F}$	τ (fs)	B(M1) (μ_N^2)	B(E2) (W.u.)
	f		2607.05(11)	0	63(4)	M1			0.020^{+3}_{-3}	
	ln	2636.72(8)	535.45(5)	2101	100	0.68^{+18}_{-9}	0.022(25)	$\geqslant$1200		
$(5^-,4^-)$										
1^+	xn	2688.89(5)	802.84(8)	1885	5.1(3)	1.0^{+64}_{-64}	0.575(16)	48^{+3}_{-3}	$5.3^{+8}_{-7}\times10^{-2}$	36^{+5}_{-36}
	dng		1101.07(25)	1588	23.5(2)	–			$\leqslant$0.23	$\leqslant$68
			1849.17(7)	839	6.8(2)	1.1^{+35}_{-31}			$7.6^{+23}_{-21}\times10^{-3}$	$5.6^{+18}_{-56}\times10^{-1}$
			2688.61(10)	0	64.6(4)	M1			$3.9^{+3}_{-3}\times10^{-2}$	
4^-	xfmn	2714.94(7)	576.23(12)	2138	3(2)					
			613.71(10)	2101	97(2)	1.7^{+4}_{-3}				
						0.68^{+15}_{-9}				
4^+	xfn	2733.44(15)	403.1(6)	2330	6(3)	0.37^{+47}_{-40}	0.219(38)	220^{+60}_{-40}	0.20^{+19}_{-13}	63^{+58}_{-63}
	dfn		1100.43(5)	1632	64(4)	–			$\leqslant$0.16	$\leqslant$ 49
	fn		1145.19(7)	1588	13(4)	E2				6.2^{+38}_{-29}
	fn		1894.03(6)	839	17(3)	E2				0.65^{+30}_{-23}
5^+		2736.28(12)	920.89(6)	1815	69.3(7)	0.13^{+7}_{-8}				
			1103.35(7)	1632	30.7(7)	1.7^{+18}_{-2}				
1^+	xn	2743.5(6)	1155.8(1)	1588	13.8(3)	1.4^{+24}_{-24}	0.292(11)	150^{+10}_{-10}	$1.2^{+20}_{-12}\times10^{-2}$	6.0^{+100}_{-60}
			2743.49(11)	0	86.2(3)	M1			$1.5^{+1}_{-1}\times10^{-2}$	
3^-	x	2744.77(5)	859.26(5)	1885	38.2(3)	E1	0.078(12)	740^{+140}_{-110}	B(E1)=$3.1^{+5}_{-6}\times10^{-4}$	
			1111.67(6)	1632	12.7(2)	E1			B(E1) = $4.8^{+9}_{-8}\times10^{-5}$	
			1905.30(3)	839	49.1(3)	E1			B(E1) = $3.7^{+7}_{-7}\times10^{-5}$	
$5^{(-)}$	lfn	2747.89(12)	932.39(7)	1815	13(8)	E1	0.272(28)	170^{+30}_{-20}	B(E1) = $3.6^{+31}_{-24}\times10^{-4}$	
	fn		1114.99(6)	1632	87(8)	E1			B(E1) = $1.4^{+4}_{-3}\times10^{-3}$	
$(5,6)^-$	ln	2748.6(2)	343.5(2)	2405	22(1)	-1.8^{+36}_{-9}	0.070(48)	820^{+1930}_{-360}	$8.4^{+210}_{-80}\times10^{-2}$	$\leqslant$2800[k]
	n		647.31(7)	2101	78(1)	-0.22^{+14}_{-8}			0.19^{+17}_{-14}	8.1^{+67}_{-58}
$(6,7)^-$	dn	2759.2(1)	658.2(1)	2101	100	–	0.000(55)	$>$1060		
3^+	xfn	2766.29(4)	880.72(6)	1885	36(2)	-0.85^{+38}_{-33}	0.147(14)	360^{+40}_{-40}	$4.8^{+21}_{-16}\times10^{-2}$	16^{+7}_{-6}
	d		1133.36(7)	1632	12(4)	(1.1^{+9}_{-9})			$5.6^{+50}_{-39}\times10^{-3}$	2.1^{+18}_{-15}
			1178.06(6)	1588	39(1)	0.19^{+8}_{-7}			$3.6^{+6}_{-5}\times10^{-2}$	0.35^{+6}_{-5}
			1926.78(6)	839	13(2)	1.2^{+7}_{-7}			$1.1^{+8}_{-6}\times10^{-3}$	0.16^{+11}_{-9}
	x	2770.80(8)	669.66(2)	2101	100					
$(5,6,7)^-$										
(7^-)	x	2781.88(11)	680.61(10)	2101	100					
(2^+)	xfn	2789.17(5)	903.42(6)	1885	28(6)	0.83^{+110}_{-150}	0.200(14)	250^{+30}_{-20}	$5.1^{+63}_{-43}\times10^{-2}$	16^{+16}_{-16}
	dfn		1201.19(8)	1558	3(3)	–			$\leqslant$0.0086	$\leqslant$2.2

TABLE I. (*Continued.*)

J^π	Note	E_x (keV)	E_γ (keV)	E_f (keV)	BR %	XL/δ[a]	$\bar{F}$	τ (fs)	B(M1) (μ_N^2)	B(E2) (W.u.)
	f		1949.72(6)	839	69(7)	-1.6^{+11}_{-11}			$6.2^{+52}_{-45} \times 10^{-3}$	1.5^{+13}_{-11}
(5^+)	xg	2833.41(21)	(501.7(6))	2330	[5.3(7)][r]	–				
	d		1018.04(6)	1815		–				
					[84.5(16)][r]					
	d		1200.77(20)	1632		–				
					[10.1(13)][r]					
4^+	ldmn	2834.94(6)	853.51(6)	1981	71(2)	1.4^{+3}_{-4}	0.147(34)	360^{+120}_{-80}	$6.2^{+35}_{-26} \times 10^{-2}$	59^{+33}_{-25}
	n		1246.70(9)	1588	8(2)	E2				1.5^{+10}_{-7}
	n		1995.47(7)	839	21(3)	E2				0.38^{+18}_{-14}
2^+	lnm	2887.94(6)	587.85(10)	2300	11(1)	-1.4^{+43}_{-28}				
	dgn		1300.15(12)	1588	42(4)	–				
	n		2048.11(11)	839	35(1)	-1.6^{+11}_{-10}				
	n		2887.72(13)	0	12(1)	E2				
$5^{(-)}$	ldmn	2926.54(18)	490.8 (3)	2435	$\leqslant$14	-0.29^{+16}_{-14}				
	n		521.54 (6)	2405	$\geqslant$86	0.03^{+13}_{-3}				
2^+	lfmn	2945.60(5)	807.18(7)	2138	12(3)	0.19^{+30}_{-26}	0.180(19)	290^{+40}_{-40}	$4.4^{+20}_{-16} \times 10^{-2}$	0.89^{+40}_{-89}
	fn		1059.87(7)	1885	16(1)	1.4^{+9}_{-32}			$9.3^{+240}_{-7} \times 10^{-3}$	5.7^{+48}_{-57}
	fn		2106.24(11)	839	46(2)	-0.51^{+28}_{-28}			$7.8^{+26}_{-21} \times 10^{-3}$	0.17^{+6}_{-5}
	fn		2945.59(11)	0	26(2)	E2				0.086^{+20}_{-16}
3^+	ldn	2953.24(14)	1320.14(8)	1632	20(2)	–	0.218(34)	220^{+50}_{-40}	$\leqslant 3.0 \times 10^{-2}$	$\leqslant$6.2
	dgn		1365.85(37)	1588	14(3)	–			$\leqslant 2.1 \times 10^{-2}$	$\leqslant$4.0
	n		2113.93(11)	839	66(3)	-0.82^{+32}_{-26}			$1.1^{+5}_{-4} \times 10^{-2}$	0.58^{+29}_{-20}
(4^+)	ldmnx	2956.7(5)	1323.3(5)	1632	16(2)	–	0.078(35)	740^{+650}_{-250}	$\leqslant 9.1 \times 10^{-3}$	$\leqslant$1.9
	nd		1368.6(9)	1588	9(1)	E2				0.53^{+37}_{-29}
	n		2117.2(2)	839	75(4)	E2				0.50^{+30}_{-25}
(7^-)	lng	3006.4(3)	905.2(3)	2101	100					
5^+	ln	3021.21(13)	1039.78(6)	1981	100	0.37^{+25}_{-15}	<0.040	$\geqslant$1500	$\leqslant$0.032	$\leqslant$1.6
$(5,6)^-$	ln	3036.75(12)	400.21(21)	2636	52(2)	-0.73^{+45}_{-53}	0.072(100)	$\geqslant$300[k]	$\leqslant$1.3	$\leqslant$1700[k]
	n		935.46(6)	2101	48(2)	3.1^{+14}_{-14}			$\leqslant$0.016	$\leqslant$67
(5)	ln	3046.6(2)	1231.03(6)	1815	71(3)					
	n		1414.14(10)	1632	29(3)					
(4,2,3)	lmn	3055.4(4)	289.1(2)	2766	100	-0.06^{+19}_{-14}				
(0-4)	lmn	3083.10(12)	2243.61(11)	839			0.254(45)	190^{+60}_{-40}		
2^+	ln	3094.82(13)	956.34(7)	2138	7.4(3)	0.16^{+23}_{-17}	0.263(20)	180^{+20}_{-20}	$2.6^{+5}_{-5} \times 10^{-2}$	0.27^{+6}_{-27}
	dn		1209.35(50)	1885	3.1(3)	–			$\leqslant 7.0 \times 10^{-3}$	$\leqslant 1.4^{+4}_{-3}$

TABLE I. (*Continued.*)

J^π	Note	E_x (keV)	E_γ (keV)	E_f (keV)	BR %	XL/δ[a]	$\bar{F}$	τ (fs)	B(M1) (μ_N^2)	B(E2) (W.u.)
	dn		1461.70(8)	1632	27.6(2)	E2				4.9^{+7}_{-6}
	n		1506.68(6)	1588	18.2(6)	-1.6^{+13}_{-12}			$\leqslant 8.6 \times 10^{-3}$	2.0^{+20}_{-17}
	n		2255.32(11)	839	26.5(8)	-1.5^{+7}_{-8}			$2.4^{+13}_{-21} \times 10^{-3}$	0.37^{+26}_{-19}
	n		3094.8(5)	0	17.2(6)	E2				0.072^{+12}_{-10}
6^-	lmn	3103.67(8)	1002.40(6)	2101	100	-0.68^{+28}_{-65}	0.037(102)	$\geqslant 400$		
1	ldmn	3110.01(18)	1521.74(6)	1588	21(2)	–	0.136(27)	390^{+120}_{-80}		
	n		2270.94(14)	839	16(1)	–				
	n		3110.08(51)	0	63(2)					
2^+	ldmn	3128.76(13)	938.28(6)	2190	14.2(8)	-1.5^{+13}_{-13}	0.039(45)	$\geqslant 680$		
	n		990.49(10)	2138	11.9(8)	0.09^{+320}_{-320}				
	n		1243.08(6)	1885	17.4(6)	0.73^{+86}_{-97}				
	n		1540.39(11)	1588	11.1(7)	0.59^{+81}_{-77}				
	n		2289.30(12)	839	21.9(8)	-1.5^{+17}_{-18}				
	n		3128.78(51)	0	23.5(9)	E2				
$(6,7)^{(-)}$	ln	3132.15(8)	1030.88(6)	2101	100	1.7^{+7}_{-9}	0.089(62)	630^{+1600}_{-280}	$2.1^{+37}_{-18} \times 10^{-2}$	21^{+32}_{-18}
(5^+)	ldn	3137.8(3)	1322.42(10)	1815	100	0.93^{+130}_{-110}				
(5,6,7)	ldn	3144.8(3)	998.71(12)	2146	100					
4^+	xd	3154.52(7)	1521.64(6)	1632	27(2)	-0.36^{+25}_{-29}	0.182(31)	280^{+70}_{-50}	$1.4^{+6}_{-5} \times 10^{-2}$	0.28^{+12}_{-9}
	n		1566.04(15)	1588	13(1)	E2				1.0^{+4}_{-3}
	n		2314.83(11)	839	60(2)	E2				0.67^{+18}_{-16}
(5,3)	lmn	3163.4(2)	1181.97(11)	1981	100	-2.3^{+18}_{-10} -0.36^{+25}_{-29}				
3^-	lnx	3176.90(7)	1075.76(6)	2101	28(1)	E2	0.086(78)	660^{+7000}_{-340}		6.2^{+72}_{-57}
	n		1291.21(6)	1885	61(1)	E1			$B(E1) = 1.6^{+18}_{-15} \times 10^{-4}$	
	n		2337.34(14)	839	11(1)	E1			$B(E1) = 5.0^{+54}_{-46} \times 10^{-6}$	
$(5^-, 7^-)$	ln	3181.16(9)	1079.90(7)	2101	100	0.40^{+40}_{-38}				
4^-	ln	3187.71(8)	1086.44(6)	2101	100	1.1^{+5}_{-6}	0.054(51)	1100^{+3900}_{-600}	$1.8^{+32}_{-15} \times 10^{-2}$	7.2^{+120}_{-62}
0-4	lmn	3195.24(13)	1309.66(14)	1885	38(4)					
	dgn		1607.04(21)	1588	62(4)					
2^+	ldgn	3196.28(15)	1057.61(22)	2138	4(1)	–	0.334(29)	130^{+20}_{-20}	$\leqslant 0.022$	$\leqslant 7.1$
	dgn		1608.16(8)	1588	24(4)	–			$\leqslant 3.5 \times 10^{-2}$	$\leqslant 4.9$
	n		2356.60(16)	839	16(5)	0.59^{+77}_{-64}			$4.1^{+29}_{-26} \times 10^{-3}$	0.094^{+73}_{-94}
	n		3196.13(51)	0	56(8)	E2				0.28^{+8}_{-8}
3,(2)	ldmn	3204.6(1)	369.95(22)	2835						
	dn		1066.04(6)	2138						

TABLE I. (*Continued.*)

J^{π}	Note	E_x (keV)	E_{γ} (keV)	E_f (keV)	BR %	XL/δ[a]	$\bar{F}$	τ (fs)	B(M1) (μ_N^2)	B(E2) (W.u.)
	dn		1318.84(14)	1885						
	dn		1616.56(12)	1588						
(1-4)	lmn	3236.3(2)	2396.81(18)	839	100					
$(4,6)^-$	ln	3236.82(8)	1135.55(6)	2101	100	1.1^{+6}_{-6}				
1	lmn	3241.73(51)	3241.73(51)	0	100		0.216(32)	230^{+50}_{-40}		
3^-	ldn	3243.48(10)	1142.2(3)	2101			0.300(50)	140^{+40}_{-30}		
	n		1357.95(15)	1885	$\leqslant$19.4					
	n		2403.94(12)	839	$\leqslant$80.6					
(5)	ldn	3287.6(3)	851.6(2)	2435						
(4,3,2)	lgmn	3319.1(2)	1433.46(8)	1885	–		0.172(117)	300^{+760}_{-150}		
	ng		1731.2(5)	1588	–					
	n		2479.7(2)	839						
(3^+)	lmn	3340.5(2)	1752.2(2)	1588	45(5)	-0.83^{+86}_{-80}	0.265(158)	180^{+340}_{-90}		
	n		2501.4(2)	839	55(5)	0.09^{+36}_{-32}				
(3,4)	lmn	3342.9(2)	1710.2(2)	1632	28(3)	–				
	n		1754.4(2)	1588	72(3)	1.2^{+16}_{-15}				

[a] When two mixing ratios are possible, the solution with the lowest χ^2 value is listed first. Multipole-mixing ratios and B(XL)s presented are for the first spin listed when the spin of the initial state is not definite.
[b] Adopted value from Ref. [18].
[c] $B(E2) = 14.9(5)$ W.u. from Ref. [21].
[d] Doublet.
[e] The angular distribution for the data set at 3.3 MeV incident neutron energy has two solutions for the multipole-mixing ratio with the second δ = -0.26(7), which agrees with Ref. [26].
[f] Branching ratios from excitation functions.
[g] Assignment from coincidence data.
[h] Doppler shift from $E_n = 3.3$ MeV angular distribution.
[i] Recommended upper limit (RUL) of $B(E2) < 300$ W.u. limits $\delta < 1.1$.
[j] RUL of $B(E2) <300$ W.u. limits $\delta < 1.3$.
[k] RUL of $B(E2) < 300$ W.u. limits $\tau > 1.4$ ps for the 2748.6 keV level, and $\tau > 1.2$ ps for the 3036.7 keV level.
[l] New level.
[m] Statistical model calculations show strength is probably missing from this level as branching ratios, while consistent, do not align with calculations for the preferred spin from the angular distributions. This observation could indicate an unassigned decay or that the level is not well described by the statistical model.
[n] New transition.
[r] Branching ratios from Ref. [29].
[t] $B(E2) = 18(4)$ W.u. is also possible depending on the sign of the $E2$ matrix element used in shell model calculations of these preliminary $B(E2)$ values in Ref. [17].
[x] See text for detailed discussion.

of the excitation function of the 330.7 keV γ ray with SMC further supports J = 7 for this level.

2300.1 keV $(1^+, 2^+)$ *level.* The angular distributions of the weak ground-state decay and strong decay into the 2_1^+ state are not of sufficient quality to distinguish between J = 1 and J = 2 for this level. Comparisons of excitation functions with SMC prefer J = 1, as shown in Fig. 3(a). The level was given a tentative (2^+) assignment in Ref. [26] from a positive a_2 value, and it was also considered as a possible lowest 2^+ mixed-symmetry state in ^{130}Te [27]. This level was previously reported from INS studies [52] as a candidate for the lowest-lying 1^+ state in ^{130}Te based on a negative a_2 and systematic trends of lifetimes and B($M1$; $1_1^+ \rightarrow 0_1^+$) values across the stable Te isotopic chain. Neither spin can be dismissed definitely because of the large uncertainty in the negative a_2 observed in this work, although J = 1 is preferred.

2330.7 keV 4^+ *level.* This level has previously been assigned 697.7 and 1491.2 keV de-exciting γ rays and has an adopted $J^\pi = (4^+)$. New angular distributions for these γ rays support the J = 4 spin assignment. A third γ ray of 349.3 keV is newly assigned to this level through its strong presence in Gate(348). Branching ratios listed in Table I were deduced by using the SMC iteratively until a consistent description of the angular distributions and excitation functions for this $J^\pi = 4^+$ level was obtained, since the 349.3 keV γ ray cannot be resolved from the much stronger 348.5 keV γ ray from the 1981.4 keV level [18].

2405.0 keV 6^- *level.* This level has an adopted $J^\pi = (6)^-$ [18]. The angular distribution of the decay to the 5_1^- state observed in these measurements allows J = 3, 4, 6, (5), while that of the decay to the 7_1^- level strongly supports J = 6 with a nonzero multiple-mixing ratio. Comparisons of SMC with γ-ray excitation functions for this level supports J = 5 or 6, leaving J = 6 as the most consistent level spin assignment.

2432.3 keV $(6^+, 7^-)$ *level.* The adopted spin and parity of this level are $J = (7)^-$. The angular distribution of the 286.2 keV γ ray supports J = 5, 6 and that of the 331.1 keV γ ray prefers J = 3, 4, 6; however, the doublet nature of the latter γ ray limits the analysis. For J = 6, the minima in the χ^2 versus $\tan^{-1}(\delta)$ curves indicate no multipole mixing is required to describe either decay. Previous $(n, n'\gamma)$ reactor-based measurements reported this level as $J^\pi = (7^-)$ [26] with an $a_2 = -0.16(6)$ and $a_4 = 0.00(8)$, which agrees well with our $a_2 = -0.12(3)$ and $a_4 = -0.01(4)$. This level was seen in the β decay of the (8^-) state in ^{130}Sb which populated 7^-, 8^-, 9^- states directly [28], but it is fed in the level scheme developed in that report. It is also labeled as a 7^- level without discussion in deep inelastic $^{130}\mathrm{Te} + {}^{64}\mathrm{Ni}$ reaction measurements [33]. Results from our new INS measurements prefer $J^\pi = 6^+$, which seems consistent with 6_2^+ energies across the Te isotopic chain [18], but $J^\pi = (7)^-$ cannot be ruled out.

2449.4 keV 4^+ *level.* A 861.6 keV γ ray [18] has been reported only in results from a β-decay experiment [29]; it is weakly observed in this work but with a threshold greater than 2.6 MeV. The angular distribution of the 816.4-keV γ ray is consistent with the adopted J = 4. A new 467.9-keV γ ray is assigned to this level from coincidence data; this γ ray is unresolved from the much stronger 468.3 γ ray from the $5_1^- \rightarrow 6_1^+$ decay. The excitation function of the 816.4-keV γ ray is consistent with the 4^+ SMC for an 80% branch; therefore, branches of 80(4)% and 20(4)% are estimated for the 816.4-keV and 467.9-keV γ rays, respectively. In the β decay study of Ref. [29], a 468.0 keV γ ray is observed that is assigned to the 2101-keV 5^- level; this would be a rather strongly forbidden transition since the level scheme reported does not indicate feeding of the 5_1^- state from higher levels. If the intensity of the 816.3- and 468.0-keV γ rays of Ref. [29] are used, then the branching ratios would be 79(2)% and 21(2)%, respectively, in excellent agreement with our INS measurements.

2466.9 keV 2^+ *level.* γ rays from this level are observed with energies of 581.1 (new), 878.7 (new), 1627.4, and 2466.9 keV. The adopted $J^\pi = 2^+$ is supported by all angular distributions and all transitions are seen in the appropriate coincidence gates; however, SMC indicate that strength is missing from this level, where missing strength is defined by footnote m in Table I.

2527.1 keV 3^- *level.* Three new γ rays are observed for this adopted $J^\pi = 3^-$ state [18]. The excitation functions of all γ rays belonging to this state are significantly greater than SMC for all possible spins, but in a consistent way; this typically indicates a state is not well described by a statistical model calculation. This state was not seen in early proton scattering measurements that reported the lowest collective octupole-vibrational strength at 2.73 MeV [39,40,42,45]; however, it was observed in reactor-based $(n,n'\gamma)$ measurements [26].

2575.0 keV 3^+ *level.* Three γ rays are observed from this level, which was previously observed in $\beta\gamma$ coincidence [30]: 942.0, 986.7 (new), and 1735.7 (new) keV, and all support J = 3 for the level spin and have nonzero $E2/M1$ multipole-mixing ratios. Unassigned 942.2 and 985.4 keV γ rays are reported in the β decay study of Ref. [29] that observed mostly states with $J^\pi = 4^+, 5^+, 6^+$ directly. All γ rays observed in these new results have negative a_2 coefficients, which do not support $E2$ transitions into the 2_1^+ and 2_2^+ states, so J = 4 is eliminated as a possible level spin, and the large angular momentum transfer required for J = 5 or J = 6 is not supported in this work. [Note: The 986.7 keV γ ray is just negative with an $a_2 = -0.001(0.038)$.]

2581.0 keV 2^+ *level.* This level has a tentative adopted [18] spin and parity of $J^\pi = (2^+)$. The angular distribution of the 992.8 keV γ ray supports J = 2, 3, 4 with similar χ^2, while the angular distribution of the 1741.5 keV γ ray prefers J = 4, but does not exclude J = 2 or 3. The excitation function data are above the SMC, but closest to J = 2 making this the most likely spin.

2607.2 keV $1^{(+)}$ *level.* Along with the known γ rays, a new decay to the 2_3^+ state is observed for this adopted J = 1 level [18]. Positive parity is preferred from the comparison of experimental excitation functions to SMC and trends across the stable Te isotopic chain, as the first 1^- state is expected much higher in energy and is a two-phonon quadrupole-octupole coupled state [32].

2688.9 keV 1^+ *level.* Two new γ rays are observed for this adopted level [18]. The ground-state transition confirms J = 1, and the nonzero $E2/M1$ multipole-mixing ratios for decays into 2^+ states support positive parity. This J = 1 level was observed previously in ^{130}Te(γ, γ') [32] and reactor (n, $n'\gamma$) measurements [26]. The strength of the 1101.1 keV γ-ray doublet was apportioned using $\gamma\gamma$ coincidence yields.

2714.9 keV 4^- *level.* This level is adopted [18] with a tentative $J^\pi = (4^-)$ from reactor (n,n$'\gamma$) measurements [26]. The angular distribution of the 613.7 keV γ ray strongly favors J = 4 or 6, either with nonzero multipole-mixing ratios. The newly observed 576.2 keV γ ray supports J = 2 - 5 (J = 4 with no mixing.) SMC do not describe well this level, as the experimental γ-ray production cross sections are significantly above the J = 4 calculations.

2733.4 4^+ *level and 2736.3* 5^+ *levels.* Four γ rays with energies of 405.2, 921.01, 1103.29, and 1896.9 keV are adopted from a $J^\pi = (4^+)$ level at 2736.1 keV [18]. New excitation functions and $\gamma\gamma$ coincidence gates indicate there are two separate levels: a $J^\pi = 4^+$ level at 2733.4 keV with 403.1, 1100.4, 1145.2, and 1894.0 keV γ rays and a $J^\pi = 5^+$ level at 2736.3 keV with 920.9 and 1103.3 keVγ rays. The angular distribution and χ^2 versus $\tan^{-1}(\delta)$ curve for the 1103.3 keV γ ray is shown in Figs. 5(a) and 5(b), respectively; these were used to deduce J = 5 for the 2736.3 keV level, along with the excitation function compared to SMC for the 920.9 keV γ ray shown in Fig. 3(c). The angular distributions of the 1145.2 and 1894.0 keV γ rays shown in Figs. 5(c) and 5(d) suggest J = 4 for the 2733.4 keV level. Positive parity is supported by the observation of the stronger γ rays of both levels in β-decay measurements that populated mostly $J^\pi = 4^+$, 5^+, and 6^+ levels [29].

2743.5 keV 1^+ *level.* This J = 1 level is adopted based on a ground-state decay [18], which was seen in ^{130}Te(γ, γ') [32] and reactor (n, $n'\gamma$) measurements [26]. A new 1155.8 keV γ ray is observed strongly in G(748) and is assigned to this level that has an angular distribution that limits the spin to J = 1, 2, or 3; however, the observed ground-state decay confirms unambiguously the adopted spin-1 assignment. The SMC show slightly better agreement with excitation functions for positive parity, and the transition to the 2^+_2 level has a nonzero multipole-mixing ratio.

2744.8 keV 3^- *level.* This level is adopted [18] with $J^\pi = (2^+, 3)$ and decays to the 2^+_3, 4^+_1 and 2^+_1 states were seen in reactor (n, $n'\gamma$) measurements [26]. The angular distributions of all γ rays seen in this work strongly support J = 3 with no $E2/M1$ mixing. Negative parity is assigned based on this observation, as well as the reports of a 3^- level near this energy from scattering experiments [39,40,42,45].

2766.3 keV 3^+ *level.* Four γ rays are observed from this adopted level [18]: 880.7, 1133.4, 1178.1, and 1926.8 keV. The 880.7-keV γ ray is newly assigned to this level; an adopted 949.8-keV γ ray is not observed in this work, except possibly with a threshold above $E_n = 3.3$ MeV. The adopted J^π is (4^+), possibly because the 949.8-keV transition would be to a 6^+ level [29] making spins lower than four unlikely for the level. Angular distributions indicate there are no pure decays from this level and strongly support $J^\pi = 3^+$. Because of the doublet nature of the 1133-keV γ ray, branching ratios are from the excitation functions, and the multipole-mixing ratio of this transition is tentative.

2770.8 keV $(5, 6, 7)^-$ *level.* The observed 669.7-keV γ ray has an excitation function that clearly supports a level at 2770.8 keV. This placement is further supported by peaks in Gate(468) and Gate(793). The adopted [18] 1137 keV γ ray tentatively assigned to this level from Ref. [28] is not supported in these measurements, although small contributions cannot be excluded. An 1135.6 keV γ ray is observed in this work with a threshold above $E_n = 3.1$ MeV. The angular distribution of the 669.7 keV γ ray suggests J = 3–7, with J = 7 then J = 5 slightly preferred; negative parity is supported in each case. This level was observed in the β decay of the (8^-) state in ^{130}Sb [28] with no spin indicated and in reactor (n, n$'\gamma$) measurements [26] with reported J = (6). SMC in comparison to excitation functions align well with J = 5, but combined information limits $J^\pi = (5, 6, 7)^-$.

2781.9 keV (7^-) *level.* This level is adopted with $J^\pi = (7^-)$ and 680.85(13) and 635.7(3) keV γ rays. The angular distribution of the 680.6 keV γ ray observed in these measurements supports J = 3–7, while the SMC support J = 7. An observed low-intensity 635.6 keV γ ray has neither the excitation function nor the appearance in the appropriate coincidence gates to support assignment to this level, although a very small contribution cannot be excluded. This level was observed previously in the β decay of the (8^-) state in ^{130}Sb, which supports $J^\pi = 7^-$ [28], and reactor (n, $n'\gamma$) measurements [26].

2789.2 keV (2^+) *level.* This tentatively adopted [18] level has 1156.2 and 1949.8 keV γ rays placed from reactor (n, $n'\gamma$) measurements [26]. In our new measurements, an 1155.8 keV γ ray is observed in Gate(748) and is assigned to the 2743.5 keV level; however, a 1949.7 keV γ ray is observed that clearly belongs to this level, as well as new 903.4 and 1201.2 keV γ rays. The angular distribution of the 1949.7 keV γ ray supports J = 2, 3, (1), while the angular distributions of the other two γ rays support J = 0–4. Evaluation of branching ratios is complicated because the 1201.2 keV γ ray is the weaker member of a doublet with the second member belonging to the nearby 2833.4 keV level, and the 903.4 is not well resolved from the 905.2 keV γ ray above 3.0 MeV. Excitation functions and coincidence yields were used to evaluate branching ratios. The SMC align well with the excitation functions of the 903.4 and 1949.7 keV γ rays for J = 2 for the branching ratios listed. The Doppler shifts of the 903.4 and 1201.2 keV γ rays are much smaller than that of the 1949.7 keV γ ray, which is probably due to their doublet nature. If not, then there are possibly two levels at this energy: one with J = 0 - 4 and the second with J = 3. The Doppler shift value in Table I is due only to the 1949.7 keV γ ray, which is well resolved in the data.

2833.4 keV (5^+) *level.* This adopted [18] level decays by 502.6, 1018.01, and 1200.0 keV γ rays and was assigned $J^\pi = (4, 5, 6)^+$ in Ref. [29]. The 501.7 keV γ ray observed in this work is tentatively assigned to this level through coincidence gates, and its energy is almost a keV different from the adopted value. The observed 1018.0 and 1200.8 keV γ rays are verified in coincidence and, while doublets, they have

TABLE II. Comparison of previous experimental reduced transition probabilities in ^{130}Te with values from the current (n,n$'\gamma$) measurements. Matrix elements with no uncertainties were given in Ref. [34].

$E_{\rm Level}$(keV)	J_i^π	J_f^π	B(XL)	$B(XL)_{(n,n'\gamma)}$	$B(XL)_{\rm other}$
1588	2_2^+	2_1^+	B(E2)	<19 W.u.	12(2) W.u. [17]
	2_2^+	2_1^+			3.8 W.u. [34]
	2_2^+	0_1^+	B(E2)	<0.030 W.u.	0.16 W.u [34]
1964	0_2^+	2_1^+	B(E2)	4.4(22) W.u.	0.7(2) W.u. [17]
2688	1^+	0_1^+	B(M1)	$0.039(3)\mu_N^2$	$0.022^{+28}_{-3}\mu_N^2$ [32]
2743	1^+	0_1^+	B(M1)	$0.015(1)\mu_N^2$	$0.015^{+13}_{-2}\mu_N^2$ [32]

TABLE III. $E2$ transition strengths below 6_1^+ in ^{130,132,134}Te.

Nuclide	$J_i \rightarrow J_f$	$B(E2; J_i \rightarrow J_f)$ (W.u.) Ref. [14]	SM1	SM2	Experiment	Ref.
^{130}Te	$2 \rightarrow 0$	13.9	14.0	14.0	15.1 (3)	[18]
	$4 \rightarrow 2$	14.9	16.9	17.7	14(3)	[17]
	$6 \rightarrow 4$	9.0	5.8	7.3	6.1(3)	[18]
^{132}Te	$2 \rightarrow 0$	7.7	9.1	9.0	10.8 (11)	[58]
	$6 \rightarrow 4$	5.5	3.8	3.8	3.3 (2)	[59]
^{134}Te	$2 \rightarrow 0$	4.25	5.1	5.1	5.1 (2)	[21]
	$4 \rightarrow 2$	5.0	5.3	5.8	4.3(4)	[60]
	$6 \rightarrow 4$	2.8	2.5	2.1	2.05 (4)	[60]

clear thresholds at the appropriate energy. Comparisons of SMC with γ-ray excitation functions support the J = 5 assignment if adopted branching ratios are used in the comparison.

2956.7 keV (4$^+$) level. This $J^\pi = (4^+)$ level may correspond to the 2950(20) keV level seen previously only in scattering experiments [18]. This INS study reveals 1323.3, 1368.6, and 2117.2 keV γ rays from the level, with angular distributions that together support J = 4. Statistical model calculations indicate that strength is probably missing from this level.

3154.5 keV 4^+ *level.* This tentatively adopted [18] level based on 1173 and 1522 keV γ rays was first reported in Ref. [26]. The latter γ ray is confirmed in this work, but the former, while observed, cannot be assigned unambiguously to this level. Its excitation function and lifetime differ from those of the three γ rays with energies of 1521.6, 1566.0, and 2314.8 keV assigned to this level in our work, although it cannot be excluded absolutely. The angular distribution of the 2314.8 keV γ ray supports J = 4, (2,3); the 1566.0 keV γ ray prefers J = 1,2,3,(4); and the 1521.6 keV γ ray permits J = 2–5. SMC support J = 4, which means the parity is positive due to the $E2$ transition to the 2_1^+ state. The intensity of the 1521.6 keV doublet member of this level was apportioned using coincidence data yields.

3176.9 keV 3^- *level.* The angular distribution of the 1291.2 keV γ ray into the 2_3^+ state strongly prefers J = 3 for this level; the other angular distributions support this assignment, as does the comparison of excitation functions with SMC. Negative parity is assigned based on the observed $E2$ decay to the 5_1^- state. This level may be the 3180(20) level observed previously in scattering experiments [18].

B. Comparison of experimental results

Very few electromagnetic transition rates have previously been determined for low-lying positive-parity states in ^{130}Te. Comparisons of new values with the previous measurements [17,32,34] are shown in Table II. Positive parity is assumed in Table II for the J = 1 levels. The agreement with previously measured transition rates is fair overall. The experimental results will now be compared to shell model calculations.

IV. SHELL MODEL CALCULATIONS

Shell model calculations were performed for ^{130}Te with the NuShellX@MSU code [53]. All proton and neutron single-particle orbitals in the 50–82 shell ($\pi 0g_{7/2}$, $1d_{5/2}$, $1d_{3/2}$, $2s_{1/2}$, $0h_{11/2}$) were included; this model space is designated $jj55$. The two valence protons relative to ^{132}Sn tend to occupy the $\pi 0g_{7/2}$ and $\pi 1d_{5/2}$ orbitals, while the four neutron holes tend to occupy the $\nu 1d_{3/2}$, $\nu 2s_{1/2}$, and $\nu 0h_{11/2}$ orbitals.

Two sets of interactions were employed. For the first case, referred to as SM1, the interactions (designated *sn*100) are based on the CD Bonn potential with the renormalization of the G matrix carried to third order, and a Coulomb term is added to the proton-proton interaction. Single-particle energies were set by reference to the low-excitation spectra of ^{133}Sb and ^{131}Sn for protons and neutron holes, respectively. This interaction has been used in previous works focused on the region around ^{132}Sn [22,54–56], including the recent study of Peters *et al.* [56] on ^{132}Xe, which is an isotone of ^{130}Te.

The second set of calculations, referred to as SM2, used the *GCN*50 : 82 interaction [57]. Similar to the *sn*100 interaction, it is obtained from a realistic G matrix, in this case based upon the Bonn-C potential. Various combinations of two-body matrix elements were then optimized by fitting to low-lying states in semimagic nuclei, odd-A Sb isotopes, $N = 81$ isotones, and some odd-odd nuclei around ^{132}Sn (i.e., about 400 data in 80 nuclei).

For both SM1 and SM2 the effective charges were set to $e_p = 1.7e$ and $e_n = 0.8e$ [56]. This choice was checked against the low-lying $E2$ transitions in ^{130}Te, ^{132}Te and ^{134}Te, as shown in Table III, which compares the present shell-model $B(E2)$ values below the 6_1^+ state in these three isotopes with experiment. The calculations of Teruya *et al.* [14] are also included for comparison. The present calculations are in very good agreement with each other and with experiment; they also agree quite well with the calculations of Teruya *et al.* [14].

One point of difference between the two interactions occurs for the quadrupole moment of the first excited state: SM1 predicts $Q(2_1^+) = +16.4$ e fm^2, whereas SM2 predicts $Q(2_1^+) = -4.4$ e fm^2. The experimental value from the reorientation effect in Coulomb excitation for the expected case of

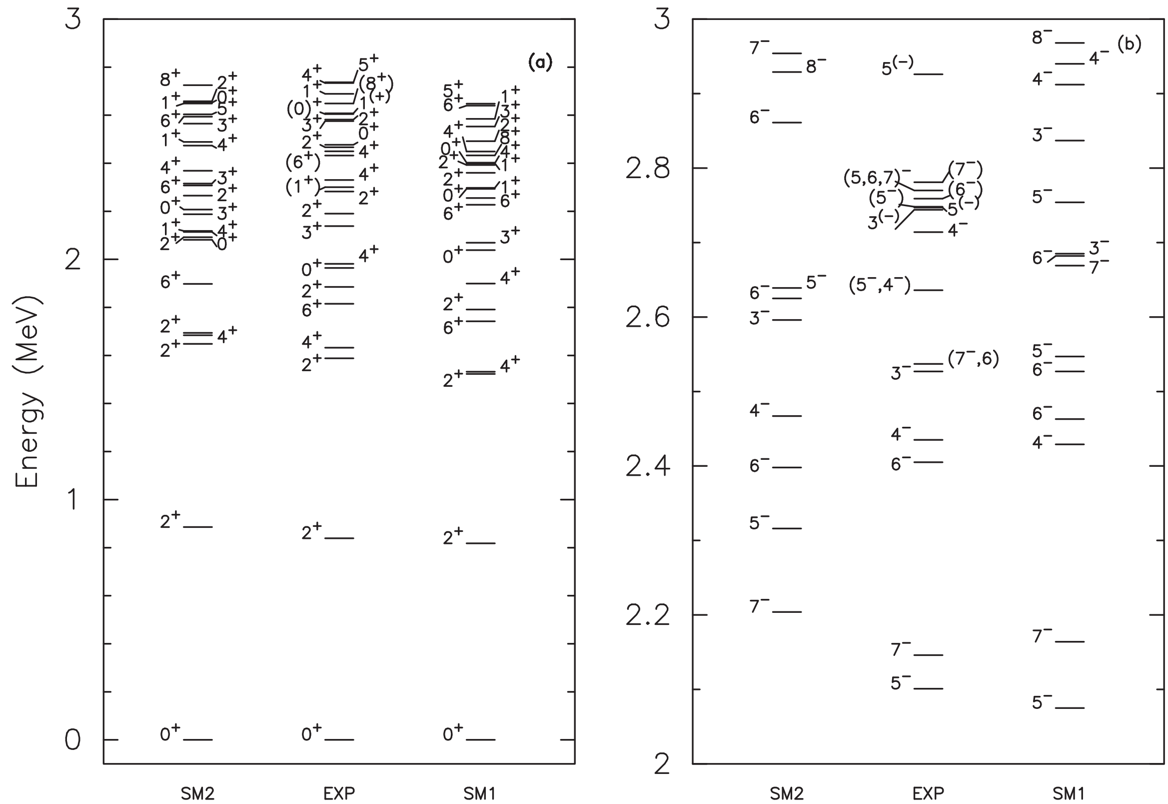

FIG. 7. Comparison of experimental level energies with shell model calculations for ^{130}Te. Positive-parity levels below 2.7 MeV are shown in panel (a) and negative-parity levels below 3.0 MeV in panel (b); note that the energy scales differ. SM1 denotes shell model calculations with the *sn100* [22,54–56] interaction and SM2 with the *GCN50:82* [57] interaction. The *jj55* model space is used in both SM1 and SM2 calculations.

a positive interference term is $Q(2_1^+) = -12(5)$ e fm^2 [61], in better agreement with SM2.

The effective $M1$ operator for both SM1 and SM2 applied a correction $\delta g_l(p) = 0.13$ to the proton orbital g factor and quenched the spin g factors for both protons and neutrons to 70% of their bare values. (The tensor term was ignored.) The effective $M1$ operator is similar to that of Jakob *et al.* [20] and in reasonable agreement with that of Brown *et al.* [22]. Previous work [21,56,62,63] has demonstrated that the chosen $M1$ operator describes well the magnetic moments of states in nuclei near $A = 130$.

V. DISCUSSION

Discussion of the shell model results and comparisons with experiment begin with the spectrum of positive-parity states below about 2 MeV in excitation energy (Sec. V A). The negative-parity states are then considered (Sec. V B). The structure of the wave functions of the low-excitation states as exposed by the calculated g factors is discussed in Sec. V C. Considerable new experimental data on $E2$ and $M1$ transition rates for nonyrast states have been obtained in the present set of experiments. These data are compared with theory, beginning with a discussion of the 2^+ states in the framework of a search for a candidate for the so-called mixed-symmetry state (Sec. V D). Detailed examinations of the electromagnetic properties of the 4^+ states (Sec. V E), and the 1^+ and 3^+ states (Sec. V F) follow. The comparison of levels and transition rates concludes with a discussion of the excited 0^+ states (Sec. V G).

Finally, an evaluation of shape invariants based on the shell model calculations and the Kumar-Cline sum rules [64,65] is presented (Sec. V H). The behavior of the deformation and triaxiality parameters for the positive-parity states gives a measure of emerging collectivity in ^{130}Te as a function of spin and excitation energy.

A. Level scheme—Positive-parity states

The experimental and theoretical level energies of ^{130}Te are compared in Fig. 7 with the positive-parity states in panel (a) and negative-parity states in panel (b). In general SM1 gives a better description of the excitation energies and level ordering than SM2. For SM1 there is good correspondence between theory and experiment for the positive-parity states from the ground state up to the first 3^+ state observed at 2139 keV. SM1 then predicts two 6^+ states and a 0^+ state. Only one possible 6^+ state at 2432 keV is observed; there is 0^+ state at 2476 keV, about 200 keV higher in energy than predicted. In both SM1 and SM2, the 6_1^+ state is predominantly associated with the $\pi(g_{7/2})^2_{6^+}$ configuration, the 6_2^+ state with $\pi(g_{7/2}d_{5/2})_{6^+}$, and the 6_3^+ state with $\nu(d_{3/2}s_{1/2}h_{11/2})^2_{6^+}$. Both SM1 and SM2 predict four 6^+ states below 3 MeV, of which two have been observed with only one of those with a firm spin assignment.

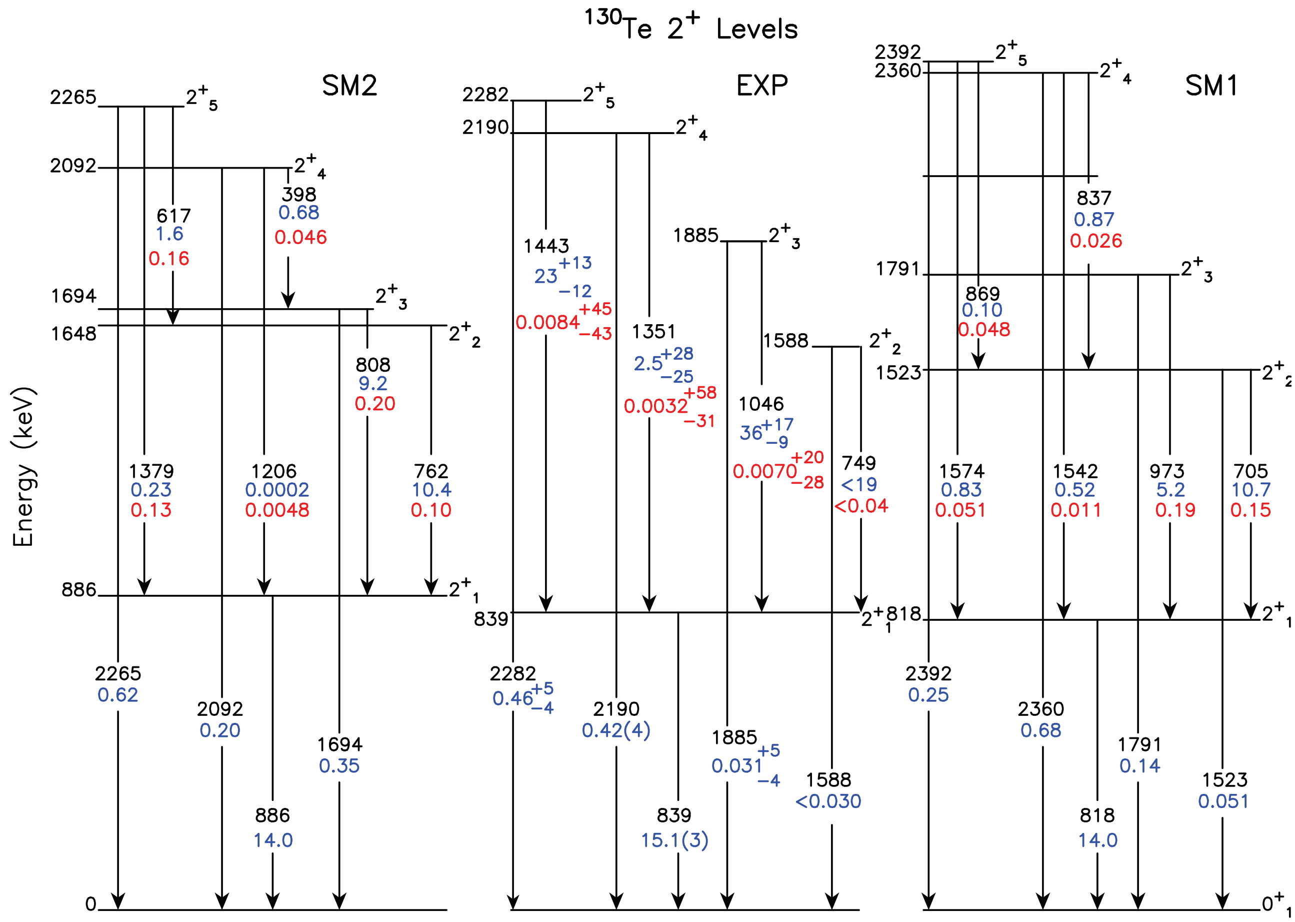

FIG. 8. The experimental decay properties of the five lowest 2^+ states in ^{130}Te compared to shell model calculations. For decays, numbers in black are γ-ray energies in keV; numbers in blue are B($E2$) values in W.u.; and numbers in red are B($M1$) values in μ_N^2. When two solutions for multipole-mixing ratios are listed in Table I, the one with the lowest χ^2 is plotted. Uncertainties are in the last digits. SM1 denotes shell model calculations with the *sn100* [22,54–56] interaction and SM2 with the *GCN50:82* [57] interaction; both sets of calculations use the *jj55* model space. Weak branches from the shell model calculations are not shown.

Above 2 MeV in excitation energy it is more challenging to identify the experimental levels with those predicted. However, in the positive-parity spectrum up to about 3 MeV there is generally a one-to-one correspondence between the number of states of each spin predicted and observed. These nonyrast positive-parity states are examined in greater detail below.

B. Level scheme—Negative-parity states

The lowest few negative-parity states are well described by the SM1 calculation, which correctly predicts that the lowest negative-parity state is a 5^- state at an excitation energy near 2.1 MeV. The structure of this state in SM1 is quite mixed but the $\nu(s_{1/2}h_{11/2})_{5^-}$ neutron configuration is strongest. The negative-parity states are not as well described by SM2, which incorrectly predicts that the 7^- state is the lowest negative-parity state.

Above 2.5 MeV in excitation energy, it becomes difficult to associate the predicted negative-parity states with particular experimental levels.

Most of the negative-parity states decay by $E1$ transitions to the positive-parity states. The calculation of $E1$ transitions requires configurations beyond those in the $jj55$ configuration space. As expected, all of the observed $E1$ transition strengths are a minute fraction of a single-particle unit.

One $E2$ transition was observed between negative-parity states, namely $B(E2; 3_1^- \rightarrow 5_1^-) = 10.4^{+61}_{-48}$ W.u. Provided we identify the SM1 shell model 3^- state at 2685 keV with the experimental 3_1^- level at 2537 keV, the predicted $B(E2) =$ 11.45 W.u. in SM1 agrees well with experiment, albeit with a significant uncertainty. The structure of the yrast 3^- level in SM1 is associated with $\nu(d_{5/2}h_{11/2})_{3^-}$, albeit with considerable configuration mixing. The $B(E2; 3_1^- \rightarrow 5_1^-)$ is comparable to the $2_1^+ \rightarrow 0_1^+$ transition strength. For both of these transitions the strength is carried about equally by protons and neutrons. This $B(E2; 3_1^- \rightarrow 5_1^-)$ value is not reproduced by SM2. Inspection of the wave functions shows that in SM1 these negative-parity states are primarily neutron excitations with a single hole in the $\nu h_{11/2}$ orbital and the other three holes in the $\nu s_{1/2}$ and $\nu d_{3/2}$ orbitals. In contrast, SM2 prefers to put three holes in the $\nu h_{11/2}$ orbital with the other hole in ether $\nu s_{1/2}$ or $\nu d_{3/2}$.

There is, therefore, a much more pronounced difference between SM1 and SM2 for negative-parity states than for positive-parity states.

TABLE IV. g factors in ^{130}Te.

State	Jakob *et al*	Teruya	Brown	SM1	SM2	Experiment [37]
2_1^+	0.445	0.146	0.341	0.343	0.310	+0.351(18)
2_2^+	0.229			0.172	0.371	
4_1^+	0.766[a]	0.515		0.594	0.643	
6_1^+	0.786[a]	0.712		0.834	0.882	

[a]Adopts a restricted basis with shell closures at $N, Z = 64$.

C. g factors and structure of the low-lying states

The theoretical g factors of the low-lying states in ^{130}Te from the present and previous shell model calculations are shown in Table IV. As well as being sensitive to the effective $M1$ operator, g factors probe the proton versus neutron contributions to the angular momentum of the state. Some of the differences in the alternative theoretical g factors for a given state in Table IV stem from the choice of the spin and orbital g factors adopted in the $M1$ operator. For example, the smaller $g(2^+)$ value of Teruya *et al.* [14] is in part due to their use of $\delta g_l(p) = 0$ in the $M1$ operator. But their calculation nevertheless implies a stronger neutron component in the 2_1^+ state than the other calculations. For example, if the operator of Teruya *et al.* is used in SM1, then it gives $g(2_1^+) = 0.277$, still almost twice that of Teruya *et al.* [14]. Jakob *et al.* [20] and SM1 predict a predominantly neutron character for the second 2^+ state, however there is a significant difference between the predicted $g(2_2^+)$ values for SM1 and SM2. This difference will be discussed further below.

Whereas the predictions differ for the g factors of the 2_1^+ and 2_2^+ states, the calculations all suggest increasing proton contributions in the 4_1^+ and 6_1^+ states. These features are due to persisting single-particle structure in the low-lying spectrum of ^{130}Te. Similar behavior was observed in the ^{132,134}Xe isotopes. The picture emerging from the comparison of shell model theory and experiment, for the sequence of Xe isotopes from the closed shell at ^{136}Xe to ^{132}Xe, is that collectivity begins to emerge first in the low-lying low-spin states [56]. Specifically, the 4_1^+ and 6_1^+ states become collective only with an increase in the number of valence neutron holes. It was not clear, however, if the key factor is low spin or low excitation energy, or perhaps both. This question will be considered in the following discussion.

D. Excited 2^+ states, emerging collectivity, mixed-symmetry states

The above comparisons of the level scheme and electromagnetic observables for the lower-lying states show overall general agreement between the shell model calculations and the experimental data at low excitation energies. The present experiments have led to a wealth of new information on the electromagnetic decays of higher-lying states to which attention will now be turned. It is convenient to begin with the 2^+ states. The recent work of Peters *et al.* [56] on the Xe isotopes suggested that quadrupole collectivity in ^{132}Xe was emerging beginning with the 2_1^+ state and building up to higher excitation energies and spins. This conclusion was based on comparisons of shell model calculations with experimental data including $E2$ transition strengths and excited-state g factors as the number of neutron holes increased away from the closed shell at ^{136}Xe. The shell model calculations showed fragmentation of the wave functions into many components and evidence that these many components were, on average, adding coherently to enhance $E2$ transition strengths. For the Te isotopes, extensive data similar to that for the Xe isotopes is not yet available. However, the present experiments have produced considerable data on transition rates for higher-lying states, particularly 2^+ states. One possible way to view emerging collectivity is to search for evidence of interacting boson model type mixed-symmetry structures developing in the low-lying 2^+ states. Mixed-symmetry states have been investigated previously in ^{130}Te with these data [27]; we examine them again guided by the new shell model calculations.

The present shell model calculations of the 2^+ states up to the 2_5^+ state are compared with experiment in Fig. 8. Excitation energies, $B(E2)$, and $B(M1)$ values are indicated. Bianco *et al.* [24], in their shell-model-based study of mixed-symmetry states in ^{130}Te, also calculated the decay properties of the low-lying 2^+ states. Their results for $E2$ decays are compared with the present calculations and experiment in Table V. The present calculations for the $M1$ decay strengths in the $2_i^+ \to 2_1^+$ transitions ($1 < i \leqslant 6$) are compared with experiment in Table VI. To assess the sensitivity of the $M1$ transition strengths to the parameters of the $M1$ operator, the $M1$ transitions in Table VI were evaluated with both the bare $M1$ operator and the effective operator that describes well the magnetic moments of states in nuclei near ^{132}Sn. Use of the

TABLE V. $B(E2)$ decay strengths from 2^+ states to the ground and first-excited states of ^{130}Te. Small deviations from Ref. [27] are from a reanalysis of the data and supersede previous results. If multipole-mixing ratios have not been uniquely determined, then two results are given for the respective transition strengths (see text).

		$B(E2; I_i \to I_f)$ (W.u.)			
E_i (keV)	$I_i \to I_f$	Bianco	SM1	SM2	Experiment
$2_i^+ \to 0_1^+$ transitions					
839	$2_1^+ \to 0_1^+$	13.6	14.0	14.0	15.1(3) [18]
1588	$2_2^+ \to 0_1^+$	0.02	0.05	0	<0.030
1886	$2_3^+ \to 0_1^+$	0.002	0.14	0.35	0.031^{+5}_{-4}
2190	$2_4^+ \to 0_1^+$	0.37	0.67	0.20	0.42(4)
2283	$2_5^+ \to 0_1^+$	0.002	0.25	0.62	0.46^{+5}_{-4}
2467	$2_6^+ \to 0_1^+$	0.05	0.048	0.0007	0.031(5)
$2_i^+ \to 2_1^+$ transitions					
1588	$2_2^+ \to 2_1^+$	3.4	10.7	10.4	<19, 12(2) [17]
1886	$2_3^+ \to 2_1^+$	0.003	5.2	9.15	36^{+17}_{-9}
					1.3(2)
2190	$2_4^+ \to 2_1^+$	10.3	0.51	1.7×10^{-4}	2.5^{+28}_{-25}
2283	$2_5^+ \to 2_1^+$	5.2	0.82	0.22	23^{+13}_{-12}
					0.60(4)
2467	$2_6^+ \to 2_1^+$	0.34	0.09	0.27	1.8^{+50}_{-18}
					0.37(8)

TABLE VI. $B(M1)$ decay strengths from 2^+ states to the first-excited state of ^{130}Te. Small deviations from Ref. [27] are from a reanalysis of the data and supersede previous results. If multipole-mixing ratios have not been uniquely determined, then two results are given for the respective transition strengths (see text).

		$B(M1; J_i \to 2_1^+)$ (μ_N^2)				
		SM1		SM2		
E_i (keV)	J_i	bare	eff	bare	eff	Experiment
1588	2_2^+	0.079	0.147	0.045	0.101	<0.040
1886	2_3^+	0.086	0.193	0.110	0.203	$7.0^{+20}_{-28} \times 10^{-3}$
						0.11(2)
2190	2_4^+	0.014	0.011	0.003	0.005	$3.2^{+58}_{-31} \times 10^{-3}$
2283	2_5^+	0.091	0.051	0.199	0.134	$8.4^{+45}_{-43} \times 10^{-3}$
						0.13(7)
2467	2_6^+	0.0026	9.6×10^{-4}	0.047	0.032	$4.7^{+120}_{-47} \times 10^{-5}$
						0.010(3)

effective operator can change the $M1$ transition rate by a factor of two—sometimes increasing it and sometimes decreasing it. The $M1$ transition rates for SM1 and SM2 are generally within a factor of two of each other.

Before discussing the comparison of theory and experiment in more detail, it is worth noting that for most of the $2^+ \to 2^+$ transitions in Tables V and VI, the multipole-mixing ratios have not been uniquely determined. $B(E2)$ and $B(M1)$ values determined using multipole-mixing ratios with the lowest χ^2 are used in Fig. 8, while both values are listed in Tables V and VI with the lowest χ^2 value first. The level of agreement between theory and experiment is not such that firm statements can be made; however, considering both the $M1$ and $E2$ strengths, the present calculations with the effective $M1$ operator tend to favor the second listed mixing ratio, which in each case is the smaller δ in Table I, for the $2_3^+ \to 2_1^+$, $2_5^+ \to 2_1^+$, and $2_6^+ \to 2_1^+$ transitions.

The concept of mixed symmetry states (MSS) arose from the proton-neutron interacting boson model (IBM-2) [66] and has been investigated through experiment and shell model calculations in several nuclei near $N = 82$ [27,58,67], including ^{132}Te where the 2_2^+ state has been identified as the mixed-symmetry state [58]. Mixed symmetry states have also been investigated in the stable Te isotopes [27], where evidence weakly indicated a possible fragmentation of the strength between the 2_3^+ and 2_5^+ states in ^{130}Te.

In brief, the lowest-lying states in the IBM-2 are predominantly of maximum proton-neutron or F-spin symmetry ($F = F_{\max}$), while states with $F = F_{\max} - 1$, occur at somewhat higher excitation energies [66]. In this scenario the lowest 2^+ state has a proton-neutron symmetric structure that can be represented in the shell model as

$$|2_1^+\rangle = a|0_1^+\rangle_\nu|2_1^+\rangle_\pi + b|2_1^+\rangle_\nu|0_1^+\rangle_\pi + \cdots, \quad (2)$$

where the kets with subscripts π and ν represent the excitations in the proton and neutron subsystems, respectively. If the F-spin symmetry is applicable, then $a^2 \approx b^2 \to 0.5$ and the components represented by "$\cdots$" are small. The mixed symmetry state has the form

$$|2_{\rm ms}^+\rangle = a|0_1^+\rangle_\nu|2_1^+\rangle_\pi - b|2_1^+\rangle_\nu|0_1^+\rangle_\pi + \cdots. \quad (3)$$

Following the IBM-2 predictions, candidates for the mixed-symmetry states are typically identified by a strong (weak) $M1$ ($E2$) transition to the 2_1^+ state. It is also worth noting that the g factors of both the 2_1^+ state and the mixed symmetry $2_{\rm ms}^+$ state should have the same value, namely $g = (g(2_1^+)_\pi + g(2_1^+)_\nu)/2$, where $g(2_1^+)_\pi$ $(g(2_1^+)_\nu)$is the g factor of the first-excited state of the proton (neutron) "parent." For the case of ^{130}Te the proton and neutron parents can be associated with the semimagic nuclei ^{134}Te and ^{128}Sn, respectively. Taking $g(2_1^+)_\pi = +0.83$ and $g(2_1^+)_\nu = -0.12$, see Table VII of Brown *et al.* [22], gives $g(2_1^+) = g(2_{\rm ms}^+) \approx +0.36$, which is in agreement with the experimental g factor of the 2_1^+ state in ^{130}Te.

TABLE VII. Wave function composition and calculated g factors of 2^+ states in ^{130}Te.

State	Wave function[a]	g factor
SM1:		
2_1^+	$0.46\pi(0^+)\nu(2^+) + 0.38\pi(2^+)\nu(0^+) + 0.07\pi(2^+)\nu(2^+) + \cdots$	0.343
2_2^+	$0.45\pi(0^+)\nu(2^+) + 0.16\pi(2^+)\nu(0^+) + 0.21\pi(2^+)\nu(2^+) + \cdots$	0.172
2_3^+	$0.44\pi(0^+)\nu(2^+) + 0.23\pi(2^+)\nu(0^+) + 0.08\pi(2^+)\nu(2^+) + 0.12\pi(4^+)\nu(2^+) + \cdots$	0.353
2_4^+	$0.23\pi(0^+)\nu(2^+) + 0.49\pi(2^+)\nu(0^+) + 0.04\pi(2^+)\nu(2^+) + 0.07\pi(4^+)\nu(2^+) + \cdots$	0.819
2_5^+	$0.59\pi(0^+)\nu(2^+) + 0.15\pi(2^+)\nu(0^+) + 0.07\pi(2^+)\nu(2^+) + 0.07\pi(4^+)\nu(2^+) + \cdots$	0.307
2_6^+	$0.73\pi(0^+)\nu(2^+) + 0.05\pi(2^+)\nu(0^+) + 0.05\pi(2^+)\nu(2^+) + 0.07\pi(4^+)\nu(2^+) + \cdots$	0.103
SM2:		
2_1^+	$0.50\pi(0^+)\nu(2^+) + 0.34\pi(2^+)\nu(0^+) + 0.05\pi(2^+)\nu(2^+) + \cdots$	0.310
2_2^+	$0.34\pi(0^+)\nu(2^+) + 0.24\pi(2^+)\nu(0^+) + 0.18\pi(2^+)\nu(2^+) + \cdots$	0.370
2_3^+	$0.41\pi(0^+)\nu(2^+) + 0.25\pi(2^+)\nu(0^+) + 0.15\pi(2^+)\nu(2^+) + 0.09\pi(4^+)\nu(2^+) + 0.04\pi(2^+)\nu(4^+) + \cdots$	0.400
2_4^+	$0.64\pi(0^+)\nu(2^+) + 0.14\pi(2^+)\nu(0^+) + 0.04\pi(2^+)\nu(2^+) + 0.02\pi(4^+)\nu(2^+) + 0.04\pi(2^+)\nu(4^+) + \cdots$	0.237
2_5^+	$0.29\pi(0^+)\nu(2^+) + 0.43\pi(2^+)\nu(0^+) + 0.03\pi(2^+)\nu(2^+) + 0.08\pi(4^+)\nu(2^+) + 0.06\pi(2^+)\nu(4^+) + \cdots$	0.660
2_6^+	$0.61\pi(0^+)\nu(2^+) + 0.08\pi(2^+)\nu(0^+) + 0.08\pi(2^+)\nu(2^+) + 0.03\pi(4^+)\nu(2^+) + 0.10\pi(2^+)\nu(4^+) + \cdots$	0.128

[a]The amplitude-squared is given. Relative phases are not available.

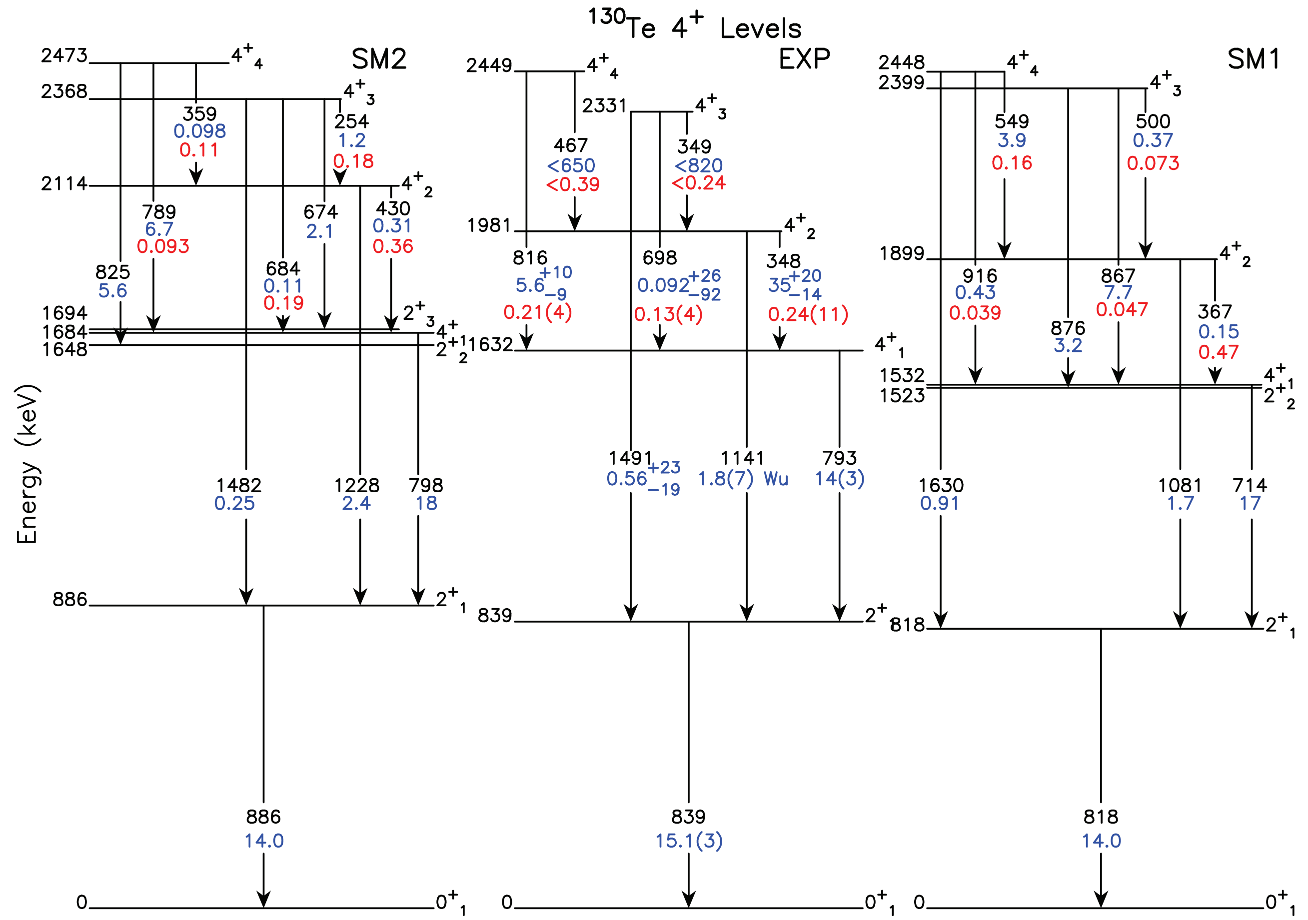

FIG. 9. The experimental decay properties of the four lowest 4^+ states in ^{130}Te compared to shell model calculations. For decays, numbers in black are γ-ray energies in keV; numbers in blue are B($E2$) values in W.u.; and numbers in red are B($M1$) values in μ_N^2. When two solutions for multipole-mixing ratios are listed in Table I, the one with the lowest χ^2 is plotted. Uncertainties are in the last digits. SM1, shown on the right, denotes shell model calculations with the *sn100* [22,54–56] interaction and SM2, shown on the left, with the *GCN50:82* [57] interaction; both sets of calculations use the *jj55* model space. Weak branches from the shell model calculations are not shown.

Table VII lists the theoretical g factors and main wave function components of the 2^+ states. It can be seen in Table VII that the structures of the 2^+_4 and 2^+_5 states are interchanged between SM1 and SM2. Such an interchange in the theory is not unreasonable as in SM1 the states are nearly degenerate and, experimentally, these states are separated by only 93 keV. Apart from this interchanged character, the main difference between the two calculations is seen in the structure and g factor of the 2^+_2 state. The proton contribution to this state is increased relative to the neutron contribution in SM2.

Overall, the comparison of theory and experiment in Tables V and VI shows that the $E2$ and $M1$ decays of the 2^+ states up to the 2^+_6 state to the ground and first-excited state generally lie near or between the predictions of SM1 and SM2 for at least one of the multipole-mixing ratio solutions. There are significant differences between the present $B(E2)$ values and those of Bianco *et al.* [24], particularly for the $2^+ \rightarrow 2^+_1$ transitions (Table V); the present shell model calculations are in better agreement with experiment.

Bianco *et al.* [24] suggested the 2^+_3 state of ^{130}Te as a possible candidate MSS because it collects a large share of the shell model $M1$ strength in their calculations, although they noted its weak $E2$ decay to the ground state is problematic. The present theory also gives a strong $M1$ to the 2^+_1, with the predicted $B(M1) \approx 0.2\ \mu_N^2$ about twice the experimental value. For SM1 the 2^+_3 wave function shown in Table VII resembles the required form and, alone among the low excitation 2^+ states in SM1, its g factor is near that of the 2^+_1 state. A cautious identification of the 2^+_3 state as a candidate MSS state seems reasonable on the basis of SM1; the properties of the 2^+_3 state are similar in SM2. This conclusion agrees with the previous report by Hicks *et al.* for the 2^+_3 state, but there is no clear fragmentation of the mixed-symmetry strength in the 2^+_5 level in the shell model calculations, although the $M1$ strength is shared in SM2. It should also be noted that experimentally the 2^+_3 state plays a very active role in the decay of higher-lying positive-parity states, which highlights its structural significance.

Although the 2^+_2 state has a wave function and g factor in SM2 that could be consistent with its being considered as a candidate for a MSS state, its small experimental $B(M1; 2^+_2 \rightarrow 2^+_1)$ and $B(E2; 2^+_2 \rightarrow 0^+_1)$ values exclude its identification as a MSS.

Thus, there are some hints of the characteristics of the MSS in the observed excited 2^+ states of ^{130}Te but no clear evidence

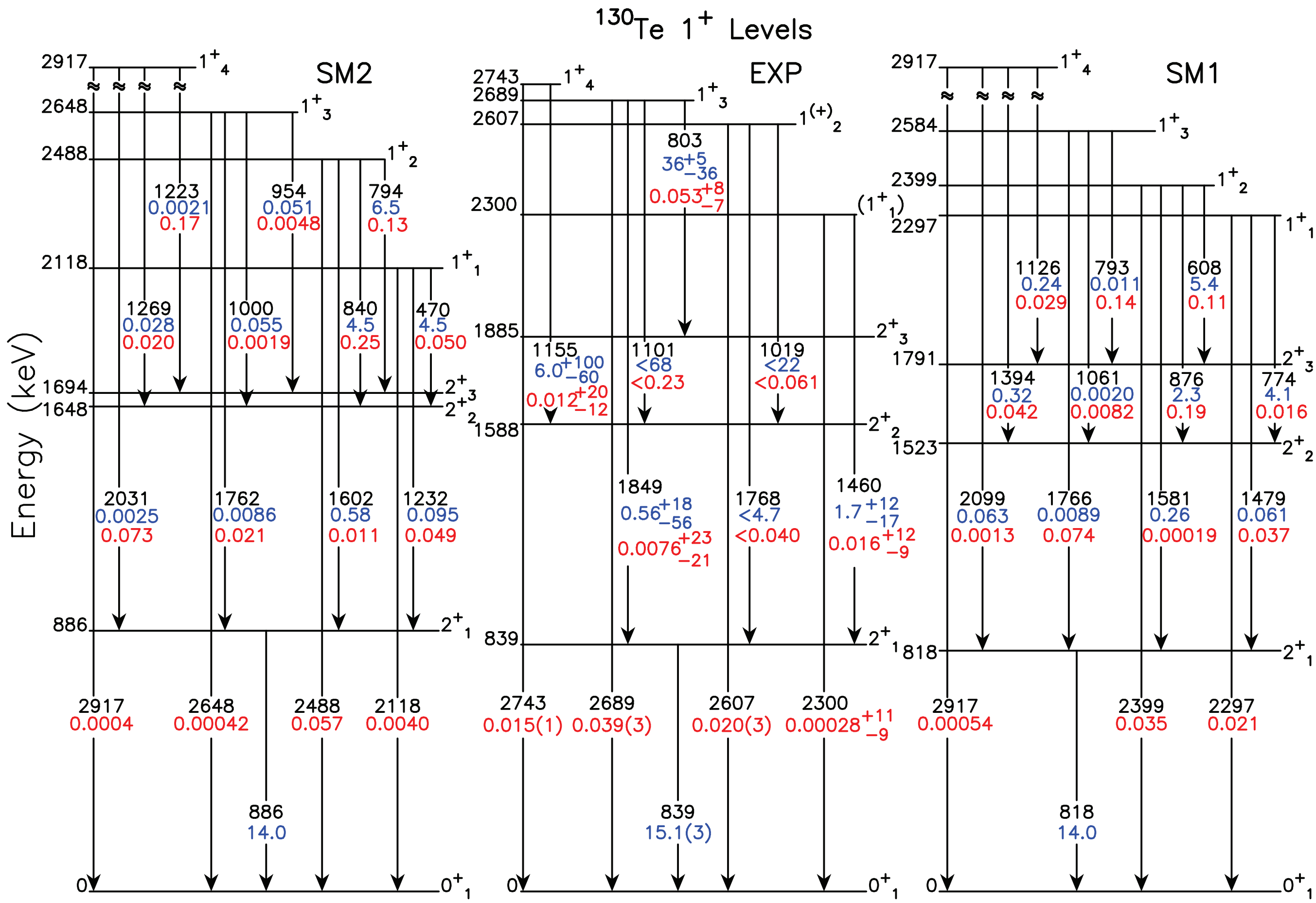

FIG. 10. The experimental decay properties of the four lowest 1^+ states in ^{130}Te compared to shell model calculations. For decays, numbers in black are γ-ray energies in keV; numbers in blue are B($E2$) values in W.u.; and numbers in red are B($M1$) values in μ_N^2. When two solutions for multipole-mixing ratios are listed in Table I, the one with the lowest χ^2 is plotted. Uncertainties are in the last digits. SM1, shown on the right, denotes shell model calculations with the *sn100* [22,54–56] interaction and SM2, shown on the left, with the *GCN50:82* [57] interaction; both sets of calculations use the *jj55* model space. Weak branches from the shell model calculations are not shown. The experimental state at 2300 keV is proposed as the 1_1^+ state, although the possibility that it is a 2^+ state cannot be excluded; see text. Shell model calculations predict the first 1^- state well above 3 MeV; however, the positive parity assigned to the 2607 keV level remains tentative.

that quadrupole collectivity in ^{130}Te is sufficiently developed to make the MSS concept based on proton and neutron bosons meaningful at a quantitative level. Addressing the question of whether collectivity builds up beginning at low spin or low energy (or both), for the larger multipole-mixing ratios for 2_3^+ and 2_5^+ states, the $E2$ strength is approximately twice the 15 W.u. $2_1^+ \rightarrow 0_1^+$ transition among the decays of the 2_2^+ to 2_6^+ states, but neither SM1 or SM2 predicts such large transition rates.

As an alternative way to assess the emergence of $E2$ collectivity in ^{130}Te, the rotational shape invariants for the low-excitation states of ^{130}Te can be calculated using the Kumar-Cline sum rules. This approach is discussed in Sec. V H below.

E. Excited 4⁺ states

The present shell model calculations of the 4^+ states up to the 4_4^+ state are compared in Fig. 9. The $E2$ decay of the 4_2^+ state to the 2_1^+ is well described by both SM1 and SM2, as is the predominantly $M1$ decay to the 4_1^+ state. Both theories predict an $E2$ decay to the 2_2^+ state with a strength of 3–5 W.u. which is not observed, perhaps because the transition energy makes this branch less favorable. SM2 describes the observed decays of the 4_3^+ and 4_4^+ states quite well; SM1 appears to swap their character, which suggests that the 4_3^+ state predicted by SM1 should be identified with the observed 4_4^+ state and vice-versa. Such an interchange is reasonable as the predicted states are within 50 keV of each other. Overall, the agreement between the shell model calculations and experiment for decays of the 4^+ states is quite good.

F. Excited 1⁺ and 3⁺ states

The experimental and theoretical decays of the lowest four 1^+ states are compared in Fig. 10. For the following discussion, and in Fig. 10, the experimental state at 2300 keV is tentatively identified as the 1_1^+ state, although the possibility that it is a 2^+ state cannot be excluded. The justification is that this is the only experimental candidate 1^+ level near the

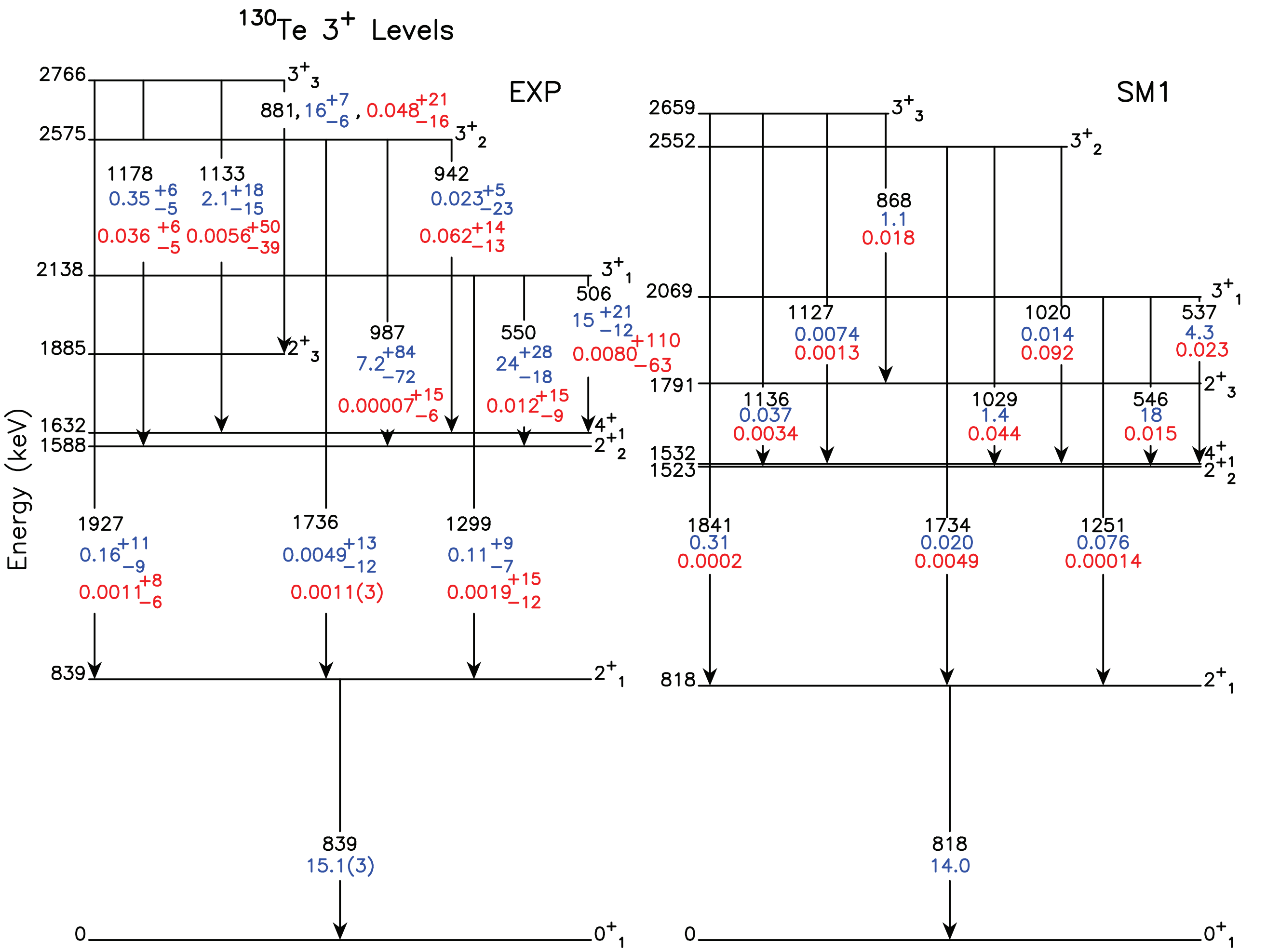

FIG. 11. The experimental decay properties of the three lowest 3^+ states in ^{130}Te compared to shell model calculations SM1 completed with the *sn100* interaction [22,54–56] and the *jj55* model space. Weak branches from the shell model calculations that are not seen experimentally are not shown. For decays, numbers in black are γ-ray energies in keV; numbers in blue are B($E2$) values in W.u.; and numbers in red are B($M1$) values in μ_N^2. When two solutions for multipole-mixing ratios are listed in Table I, the one with the lowest χ^2 is plotted. Uncertainties are in the last digits.

predictions of the shell model calculations. The 2607 keV level is tentatively identified with positive parity; the first theoretical 1^- state is near 3.4 and above 3.7 MeV for SM1 and SM2, respectively. The four lowest 1^+ states fall within 450 keV of each other. Their observed $M1$ decays are typically rather weak and in fair accord with theory for both SM1 and SM2. Where measured, the $E2$ decay strengths are also generally in fair agreement with experiment. Possible exceptions are the measured 36^{+5}_{-36} W.u. decay of the 1_3^+ level to the 2_3^+ state, and 6.0^{+100}_{-60} W.u. decay of the 1_4^+ level to the 2_2^+ state, neither of which is accounted for by theory except at their lower limits. However, 5 and 6 W.u. transitions from the 1_1^+ and 1_2^+ states to the 2_3^+ state are predicted by SM1, which suggests that appropriate configuration mixing might explain an $E2$ decay of some tens of W.u. The $M1$ decay of the 1_3^+ state to the ground state has a strength of 0.039(4) μ_N^2 and that of the 1_4^+ state to the ground state has a strength of 0.015(1) μ_N^2; both calculations predict this $M1$ strength to be orders of magnitude weaker. At the same time, both overpredict the strength of the $1_2^+ \rightarrow 0_1^+$ decay. Apparently some remixing of the 1_2^+, 1_3^+, and 1_4^+ states could account for the observed decays of these states to the ground state. Again, the states are close in energy (82 keV and 136 keV apart experimentally, respectively), so it is difficult for even state-of-the-art shell model calculations to predict the configuration mixing with sufficient accuracy to explain these electromagnetic decays in detail. It can also be noted that both shell model calculations predict the 1_5^+ state near 3.1 MeV, with the latter in good agreement with the observed J = 1 state at 3110 keV.

There are five 3^+ states observed up to 3 MeV in excitation energy. Both shell model calculations predict 3^+ states within 200 keV of those observed; in both calculations the 3_5^+ state is slightly above 3 MeV whereas the experimental 3_5^+ state is slightly below. The observed 3_2^+ through 3_5^+ states are within 400 keV of each other. Figures 11 and 12 compare the experimental and theoretical decays of the 3^+ states up to the 3_3^+ state at 2766 keV. The calculations of $M1$ and $E2$ decays of the 3_1^+ state are, on the whole, consistent with each other and with experiment. Similar behavior to that observed for the 1^+ states appears in that both calculations are in quite

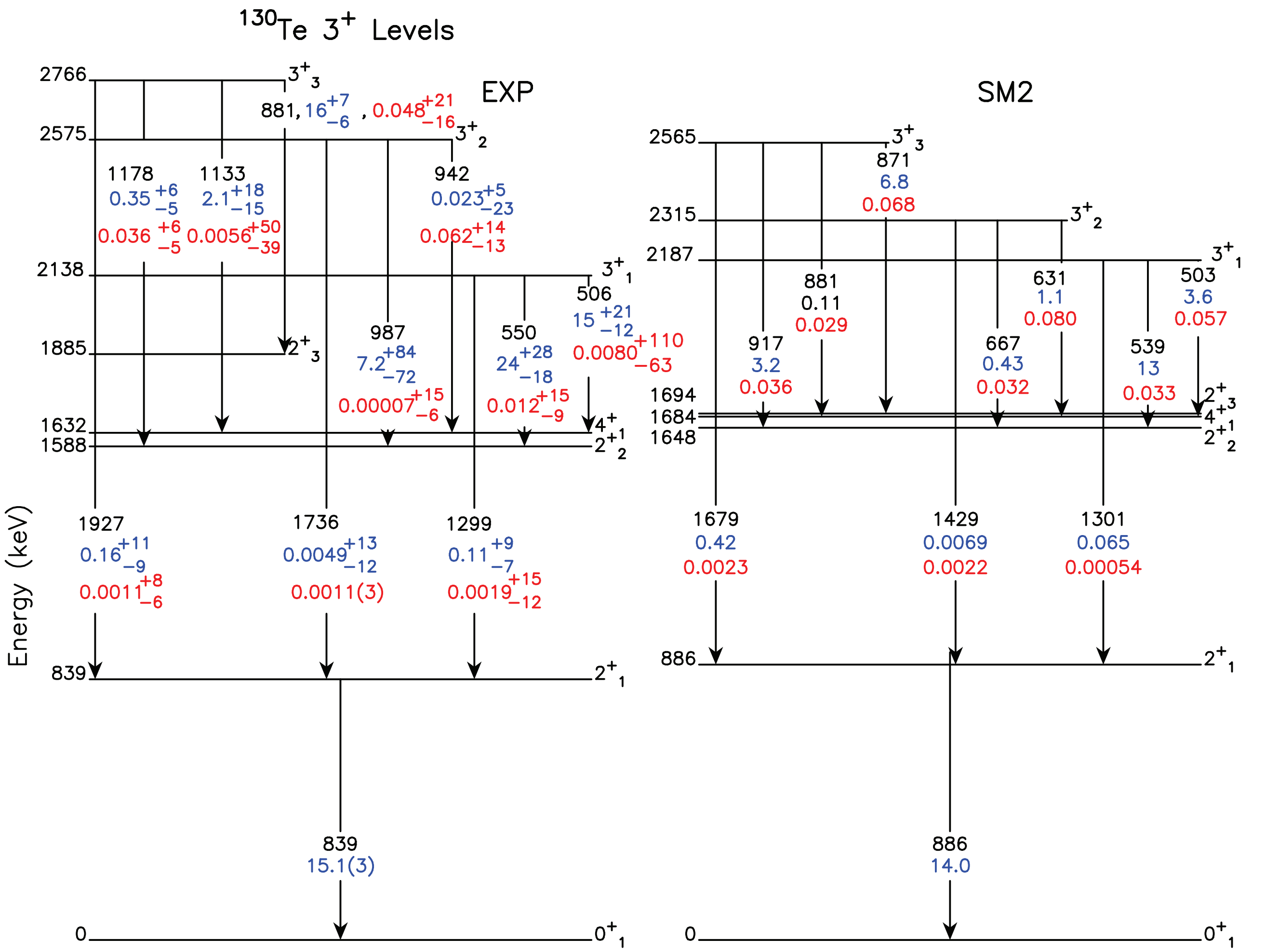

FIG. 12. The experimental decay properties of the three lowest 3^+ states in ^{130}Te compared to shell model calculations SM2 completed using the *GCN50:82* [57] interaction and the *jj55* model space. Weak branches from the shell model calculations that are not seen experimentally are not shown. For decays, numbers in black are γ-ray energies in keV; numbers in blue are B($E2$) values in W.u.; and numbers in red are B($M1$) values in μ_N^2. When two solutions for multipole-mixing ratios are listed in Table I, the one with the lowest χ^2 is plotted. Uncertainties are in the last digits.

good agreement with each other and with experiment for the decays of the 3_1^+ state, but some remixing between the higher-excited close-lying states appears necessary to improve the description of their decay.

G. Excited 0^+ states

Figure 13 shows the experimental and shell model 0^+ states in ^{130}Te along with their $E2$ decay strengths. There are four calculated 0^+ excited states below 3 MeV excitation energy for both interactions, and three candidate experimental 0^+ states, with two firmly assigned as 0^+. The 0_6^+ state is predicted to be just above 3 MeV. There is, therefore, possibly a 0^+ state in the region between about 2.5 and 3 MeV excitation energy that has not been identified in the experiment. The calculated excitation energies are not in particularly good agreement with experiment, nor are the $E2$ decay patterns, so making an association between the experimental and theoretical 0^+ levels above the 0_2^+ level is challenging.

The two shell model calculations are in agreement with experiment for the 0_2^+ state at 1965 keV, predicting that it decays almost exclusively to the 2_1^+ state, with the $B(E2)$ from SM2 perhaps in better agreement with experiment.

The branching ratios and $B(E2)$ values for the decay of the observed 0_3^+ state at 2476 keV are in very good agreement with those of the theoretical 0_5^+ state at 2693 keV in SM1. For SM2 the best agreement for the experimental 0_3^+ state is with the theoretical 0_4^+ state predicted at 2651 keV. The theoretical 0_3^+ state has very nearly 100% decay to the 2_1^+ state in both calculations, and is predicted at 2293 keV in SM1 and 2207 keV in SM2.

The decay of the experimental (0_4^+) state at 2605 keV agrees very well with the $E2$ transition strengths predicted by SM2 for the theoretical 0_5^+ state at 2887 keV; the $E2$ strengths for the 0_4^+ state at 2402 keV also agree with experiment within the uncertainties.

Thus, if a 0^+ state in the vicinity of 2.2 to 2.3 MeV excitation energy has been missed in the measurements, then there is a fair degree of agreement between theory and experiment for 0^+ states below 3 MeV in ^{130}Te.

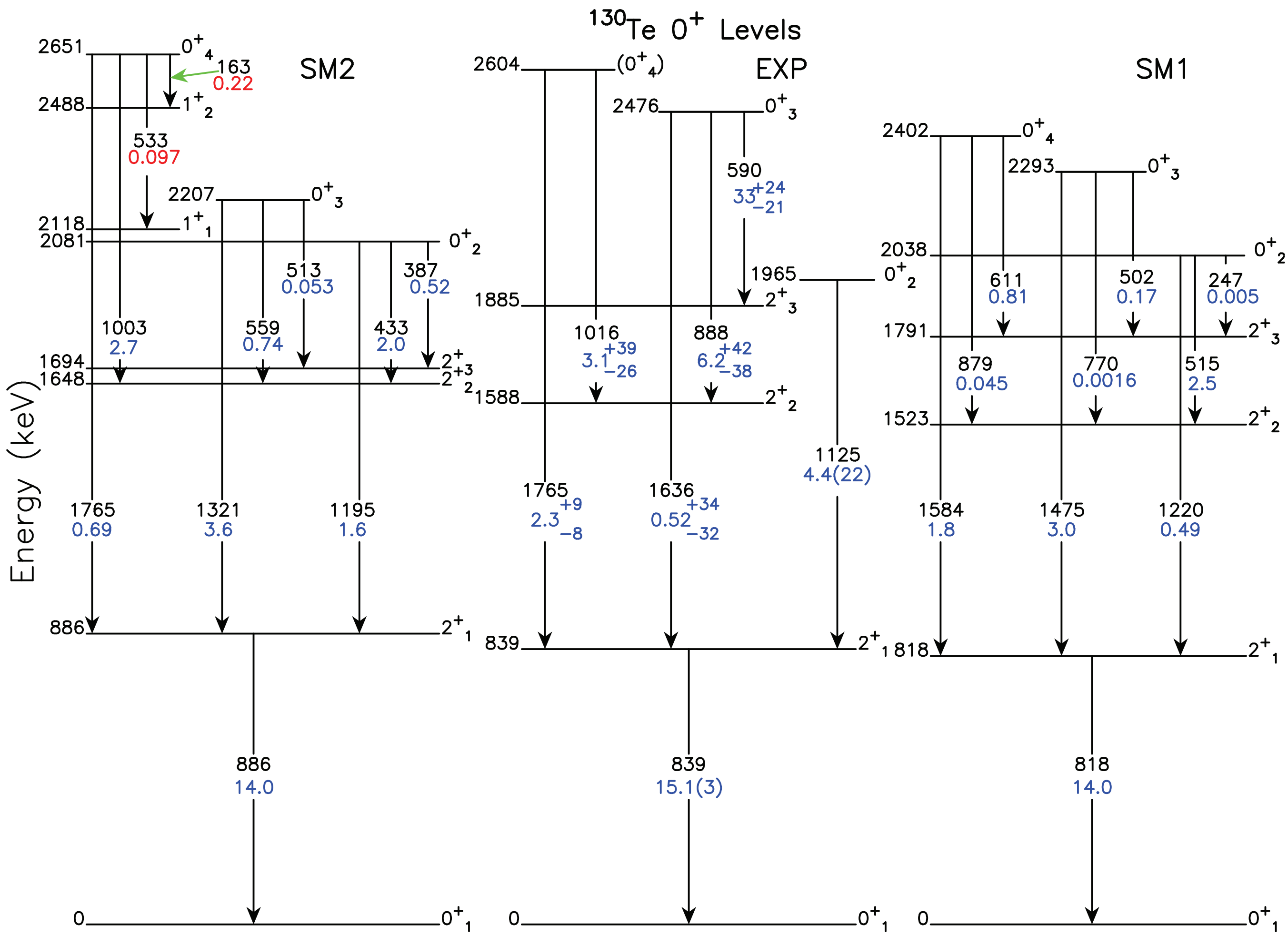

FIG. 13. The experimental decay properties of the three lowest excited 0^+ states (or candidates) in ^{130}Te compared to shell model calculations. For decays, numbers in black are γ-ray energies in keV; numbers in blue are B($E2$) values in W.u.; and numbers in red are B($M1$) values in μ_N^2. When two solutions for multipole-mixing ratios are listed in Table I, the one with the lowest χ^2 is plotted. Uncertainties are in the last digits. SM1, shown on the right, denotes shell model calculations with the *sn100* [22,54–56] interaction and SM2, shown on the left, with the *GCN50:82* [57] interaction; both sets of calculations use the *jj55* model space. Weak branches from the shell model calculations are not shown. When experimental transition rates have asymmetric uncertainties in Table I, the larger value is used in this figure.

From the pattern of excited 0^+ state systematics in the Te isotopes shown in Fig. 1, it is clear that there is a parabolic pattern of 0_2^+ excitation energies around ^{120}Te ($N = 68$), which is strongly suggestive of shape coexistence with these states built on multiparticle-multihole excitations. Nearer to $N = 82$, the above discussion and experimental data show no evidence of a shape-coexisting 0^+ state below 3 MeV in excitation energy. However, a multiparticle-multihole 0^+ state would be expected somewhat above 3 MeV, which could perturb the structures of the lower excitation 0^+ states and might, in part, account for the rather modest agreement between theory and experiment found for the low-lying 0^+ states.

H. Shape invariants as a measure of emerging collectivity

The above comparison of theory and experiment shows that the $E2$ decays of the positive-parity states up to about 3 MeV in excitation energy are generally well described by the shell model calculations using either of the interactions. In cases where a discrepancy occurs there is usually a pair of states close in energy where some remixing of the configurations or interchange of the ordering of the theoretical states would bring the theory into better agreement with experiment. In these circumstances, it seems to be well justified to use the shell model calculations of the $E2$ matrix elements to evaluate rotational invariant shape parameters based on the Kumar-Cline sum rules [64,65]. These shape invariants give a measure of the shape and shape fluctuations of the nucleus. The procedure itself is model independent. For some decades it has been applied to experimental data [65,68,69]; however, recently, there has been interest in evaluating the shape invariants from shell model calculations [70–72]. While large-basis shell model calculations may describe data well, the complexity of the wave functions can defy insight, particularly in terms of seeking signals of emerging collectivity. The advantage of the Kumar-Cline sum rules is that they provide a means to determine the nuclear shape parameters from the shell model wave functions, and thereby connect microscopic

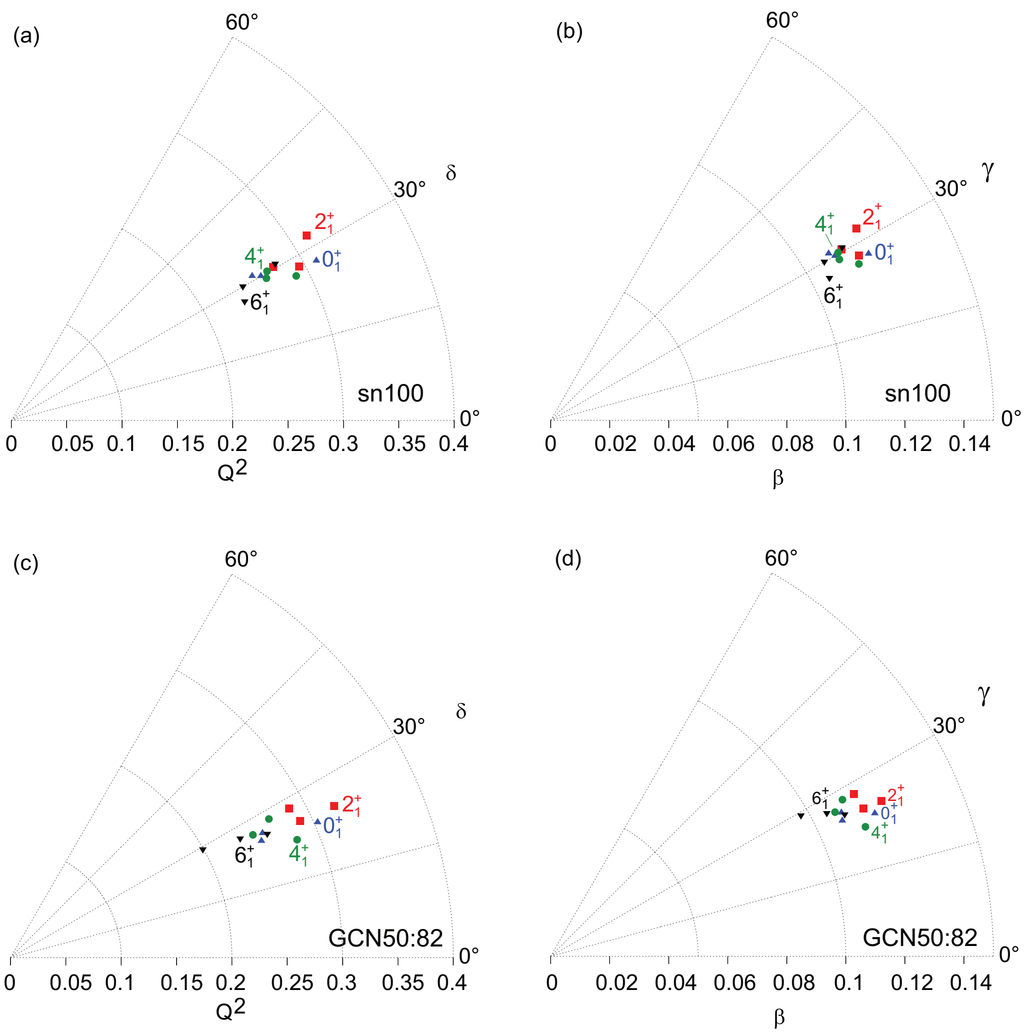

FIG. 14. Shape invariants for the low-lying 0^+, 2^+, 4^+, and 6^+ states in ^{130}Te. (a) Shape invariants (Q^2, δ) for SM1 (*sn*100 interaction), (b) the equivalent average shapes in the (β, γ) plane for SM1, (c) shape invariants (Q^2, δ) for SM2 (*GCN*50 : 82 interaction), (d) the equivalent average shapes in the (β, γ) plane for SM2.

and collective models of the nucleus. In the case of ^{130}Te this approach may provide a means to map the emergence of collectivity as a function of spin and excitation energy for the low-lying states.

The Kumar-Cline sum rules make use of the fact that the $E2$ operator is a spherical tensor that can be coupled to itself to form operator products with angular momentum zero. Such operators are rotationally invariant and can be evaluated in the principal-axis frame of the nucleus where they depend on two parameters, Q and δ, which are analogous to the Bohr model parameters β and γ. Examples are $[E2 \otimes E2]^0 = (1/\sqrt{5})Q^2$ and $[[E2 \otimes E2]^2 \otimes E2]^0 = (-\sqrt{2/35}Q^3 \cos 3\delta$. The expectation values of these invariant operators can be evaluated for each nuclear state as sums of $E2$ matrix elements by forming intermediate state expansions [65,68,69]. Q and δ can be related to β and γ in a straightforward way [68,69].

The average deformation and shape parameters Q and δ together with a measure of their fluctuations (a standard deviation, σ) were evaluated for the low-lying 0^+, 2^+, 4^+, and 6^+ states in ^{130}Te, and for both interactions. To achieve convergence, the lowest 30 states of each spin up to 12^+ were included in the relevant sums. The results, presented in the (Q^2, δ) and (β, γ) planes, are shown in Fig. 14. For clarity, the fluctuations were not plotted. They are similar in magnitude for all cases, namely $\sigma(Q^2) \sim 0.09$ and $\sigma(\delta) \sim 10^\circ$. By happenstance, therefore, the "softness" or fluctuation associated with each point is comparable to the scatter in the plotted points.

This analysis indicates that the nucleus is weakly deformed, on average, in its low-lying excited states, having $0.1 \lesssim \beta \lesssim 0.12$. A striking feature in Fig. 14 is that all of the low-lying states are triaxial. For SM1 the triaxiality parameters cluster around $\delta, \gamma = 30^\circ$, whereas for SM2 $20^\circ \lesssim \delta, \gamma \lesssim 30^\circ$.

Both interactions show the maximum deformation for the 2_1^+ state, followed by the ground state (0_1^+). The general trend is that the average deformation decreases with increases in both excitation energy and spin. But this trend is weak. Thus, the present analysis is consistent with the inference in the work of Peters *et al.* [56] on ^{132}Xe that collectivity builds up, beginning from low-lying, low-spin states. The fact that the 2_1^+ state is slightly more deformed on average than the ground state is probably because pairing correlations are more prominent in the ground state while quadrupole interactions can become more pronounced in the first 2^+ state. It would be of interest to perform a similar analysis on neighboring nuclei with added pairs of protons and/or neutron holes to investigate whether a stronger trend appears in, say, ^{128}Te or ^{132}Xe.

Do these features suggest that ^{130}Te could be modeled as a weakly deformed triaxial rotor, at least for the low-lying states up to spin 6^+? Scrutiny of the wave functions and predicted g factors in Table VII, for example, indicates that the structures of the lowest few states are very different, despite their apparently similar intrinsic shape parameters. The excitations are not rotations of a single intrinsic structure as is supposed in the triaxial rotor model. However, the fact that the excited-state shapes are all triaxial with $\gamma \approx 30^\circ$ may suggest that the pathway of emerging collectivity in this region progresses from near-spherical nuclei near ^{132}Sn, to weakly deformed triaxial rotors as an intermediate step, before finally reaching strongly deformed prolate rotors near midshell. Further data and calculations across an extended range of Te isotopes would be needed to assess this conjecture.

VI. SUMMARY AND CONCLUSIONS

The low-lying nuclear structure of ^{130}Te was investigated using γ-ray spectroscopy following inelastic neutron scattering. Many new levels and decays were identified from γ-ray angular distributions, excitation functions, and γ-γ coincidence measurements. Transition probabilities, level spins, parities, and multipole-mixing ratios were deduced for many levels. These results were investigated through new shell model calculations performed with NuShellX@MSU in the $jj55$ model space with two interactions based on the free nucleon-nucleon potential and a realistic G matrix evaluation. The positive-parity excitation energies and electromagnetic observables are well described by both the $sn100$ and $GCN50:82$ interactions. The energies of the lowest negative-parity states are also well described by the $sn100$ interactions, whereas $GCN50:82$ gives a rather poor description. The $E1$ decays of many of the negative-parity states, typically a small fraction of a single-particle unit, require the inclusion of single-particle orbitals beyond the $jj55$ space.

There is little evidence for emerging collectivity in ^{130}Te beyond the correlations included in the large-basis shell model calculations, subject to the caveat that rather large effective charges of $e_p = 1.7$ and $e_n = 0.8$ are required. Given the overall good description of the positive-parity states, the emergence of quadrupole collectivity in ^{130}Te was investigated by evaluating the rotationally invariant shape parameters of the low-lying states using the Kumar-Cline sum rules and the shell model $E2$ matrix elements. Consistent with expectations, the ground states and first-excited states showed the greatest collectivity in that they have the largest average deformations. However, all states are weakly deformed ($\beta \approx 0.1$) and triaxial. While ^{130}Te itself clearly cannot be described by a weakly deformed particle rotor model, it seems possible that triaxial structures might constitute a step in the evolution of nuclear structure from near-spherical nuclei near ^{132}Sn toward prolate rotor structures near mid shell.

The present new experimental and theoretical investigations of ^{130}Te offer nuclear structure information which may be of value for $0\nu\beta\beta$ studies. In particular, the shell model description appears on the whole to be very good. It is clear, however, that complementary measurements are needed to develop a more complete understanding of this complex nucleus and the evolution of the nuclear structure of the Te isotopes. A comprehensive Coulomb excitation measurement, for example, would be challenging but could test the prediction that the low-lying states of ^{130}Te are all weakly deformed and triaxial.

ACKNOWLEDGMENTS

This work was supported in part by the National Science Foundation Grants No. PHY0139504, No. PHY-9901508 and No. PHY-1913028, by the Australian Research Council Discovery Grant No. DP170101673, by the Office of Naval Research Naval Academy Trident Scholar Program, and by the Nancy Cain and Jeffrey A Marcus Endowment for the Sciences at the University of Dallas. We also acknowledge helpful discussions with Professor M. T. McEllistrem (deceased) of the University of Kentucky. The assistance of the accelerator engineer, H. E. Baber, is sincerely appreciated.

APPENDIX: LEGENDRE POLYNOMIAL COEFFICIENTS

Legendre polynomial coefficients for γ rays placed in ^{130}Te are listed in Table VIII. γ-ray branching ratios were determined from the A_0s, which provide the relative strengths, listed for either 2.2 or 3.3 incident neutron energy. For doublets or triplets the strength was divided using either γ-ray excitation functions or $\gamma\gamma$ coincidence data, as noted in Table I.

TABLE VIII. Legendre polynomial coefficients for γ rays placed in ^{130}Te. The A_0s give the relative strengths at the incident neutron energies (either 2.2 or 3.3 MeV) of the measurements.

E_γ (keV)	A_0	σ_{A_0}	a_2	σ_{a_2}	a_4	σ_{a_4}
$E_n = 2.2$ MeV						
182.39(20)	$1.99 \times 10^{+02}$	18.7	0.37	0.25	0.34	0.39
348.5(2)	$1.29 \times 10^{+03}$	12.8	0.38	0.03	0.04	0.04
468.3(2)	$9.65 \times 10^{+02}$	12.1	−0.23	0.04	0.09	0.05
505.62(6)	$1.95 \times 10^{+02}$	8.2	−0.60	0.12	0.19	0.17
550.30(6)	$4.38 \times 10^{+02}$	6.5	0.80	0.04	0.36	0.09
748.73(6)	$1.51 \times 10^{+04}$	33.8	0.33	0.01	−0.06	0.01
793.48(6)	$1.02 \times 10^{+04}$	12.5	0.34	0.00	−0.05	0.01
839.49(5)	$9.28 \times 10^{+04}$	58.1	0.15	0.00	−0.13	0.00
1046.15(5)	$7.10 \times 10^{+03}$	16.2	0.06	0.01	−0.05	0.01

TABLE VIII. *(Continued.)*

E_γ (keV)	A_0	σ_{A_0}	a_2	σ_{a_2}	a_4	σ_{a_4}
1125.20(5)	$1.73 \times 10^{+03}$	13.1	−0.01	0.02	−0.02	0.03
1141.93(5	$1.13 \times 10^{+03}$	10.9	0.50	0.03	−0.11	0.04
1299.07(5)	$4.42 \times 10^{+02}$	8.0	0.22	0.05	−0.14	0.08
1351.01(5)	$9.23 \times 10^{+01}$	5.5	−0.21	0.17	−0.12	0.25
1588.19(5)	$2.91 \times 10^{+02}$	7.1	0.22	0.07	−0.15	0.10
1885.70(9)	$1.17 \times 10^{+02}$	6.1	0.19	0.15	−0.19	0.22
2190.45(10)	$1.39 \times 10^{+02}$	7.4	0.70	0.15	0.10	0.22
$E_n = 3.3$ MeV						
258.83(20)	$8.89 \times 10^{+02}$	11.1	−0.47	0.04	0.10	0.05
286.23(20)	$8.04 \times 10^{+02}$	9.4	−0.12	0.03	−0.01	0.04
289.1(2)	$1.48 \times 10^{+02}$	7.9	−0.18	0.15	0.14	0.19
303.87(20)	$9.09 \times 10^{+02}$	8.3	−0.16	0.02	0.04	0.04
330.67(21)	$9.60 \times 10^{+02}$	7.6	−0.34	0.03	0.04	0.04
331.1(5)	$9.60 \times 10^{+02}$	7.6	−0.34	0.03	0.04	0.04
334.69(20)	$3.77 \times 10^{+03}$	11.4	−0.06	0.01	−0.01	0.02
343.5(2)	$1.61 \times 10^{+02}$	8.7	0.27	0.14	0.30	0.20
349.35(22)	$4.44 \times 10^{+03}$	12.1	0.24	0.01	−0.04	0.01
369.95(22)	$6.50 \times 10^{+01}$	6.3	0.26	0.28	0.56	0.38
400.21(21)	$1.58 \times 10^{+02}$	6.3	−0.04	0.12	0.06	0.16
403.1(6)	$1.19 \times 10^{+02}$	6.2	0.48	0.15	0.14	0.21
425.86(22)	$6.73 \times 10^{+01}$	6.1	0.56	0.27	0.45	0.38
436.48(21)	$1.31 \times 10^{+02}$	6.2	0.15	0.14	0.07	0.19
467.90(23)	$1.32 \times 10^{+04}$	19.0	−0.24	0.00	−0.03	0.01
490.8(3)	$1.00 \times 10^{+02}$	6.5	−0.68	0.20	−0.21	0.27
521.54(6)	$6.68 \times 10^{+02}$	8.7	−0.23	0.04	−0.02	0.05
535.45(5)	$1.23 \times 10^{+03}$	8.7	0.36	0.02	−0.04	0.03
576.23(12)	$1.11 \times 10^{+02}$	7.2	−0.54	0.21	−0.64	0.30
581.10(7)	$1.23 \times 10^{+02}$	7.2	0.10	0.18	0.20	0.25
587.85(10)	$7.04 \times 10^{+01}$	7.6	−0.30	0.33	−0.07	0.46
590.36(6)	$1.92 \times 10^{+02}$	9.4	0.16	0.15	0.03	0.21
613.71(10)	$1.79 \times 10^{+03}$	11.4	−0.58	0.02	0.03	0.03
641.44(6)	$4.39 \times 10^{+02}$	8.8	−0.18	0.06	−0.03	0.08
647.31(7)	$5.68 \times 10^{+02}$	8.8	0.27	0.05	0.04	0.06
658.2(1)	$4.37 \times 10^{+02}$	7.5	0.29	0.05	−0.07	0.07
669.66(2)	$5.93 \times 10^{+02}$	7.8	0.07	0.04	−0.27	0.06
680.61(1)	$7.12 \times 10^{+01}$	6.4	0.34	0.26	0.09	0.37
697.68(5)	$2.31 \times 10^{+03}$	10.4	0.28	0.01	0.01	0.02
802.84(8)	$8.31 \times 10^{+01}$	7.2	−0.33	0.26	−0.45	0.35
807.18(7)	$1.57 \times 10^{+02}$	7.4	−0.07	0.13	0.13	0.18
816.42(5)	$1.95 \times 10^{+03}$	10	0.18	0.02	−0.01	0.02
853.51(6)	$4.07 \times 10^{+02}$	6.9	0.18	0.05	−0.10	0.07
859.26(5)	$9.08 \times 10^{+02}$	7.4	−0.24	0.02	0.01	0.03
878.73(8)	$1.12 \times 10^{+02}$	5.5	−0.10	0.15	−0.28	0.22
880.72(6)	$3.00 \times 10^{+02}$	6.2	−0.68	0.07	−0.11	0.09
887.81(6)	$2.74 \times 10^{+02}$	5.4	0.09	0.06	0.09	0.08
894.10(6)	$1.74 \times 10^{+02}$	19.3	0.60	0.34	0.38	0.30
903.42(6)	$6.92 \times 10^{+02}$	6.9	0.43	0.03	0.19	0.04
905.2(3)	$8.36 \times 10^{+01}$	4.5	0.44	0.15	0.00	0.22
920.89(6)	$3.36 \times 10^{+02}$	5.3	−0.30	0.05	−0.06	0.07
932.39(7)	$9.03 \times 10^{+01}$	4.6	−0.10	0.15	0.06	0.21
935.46(6)	$1.48 \times 10^{+02}$	5.0	−0.43	0.10	0.07	0.14
939.1(5)	$1.53 \times 10^{+02}$	5.0	−0.24	0.10	−0.05	0.14
938.28(6)	$1.53 \times 10^{+02}$	5.0	−0.24	0.10	−0.05	0.14
942.01(5)	$1.26 \times 10^{+03}$	8.1	−0.14	0.02	−0.08	0.03

TABLE VIII. *(Continued.)*

E_γ (keV)	A_0	σ_{A_0}	a_2	σ_{a_2}	a_4	σ_{a_4}
956.34(7)	$1.11 \times 10^{+02}$	4.5	−0.09	0.12	0.10	0.17
986.74(6)	$4.45 \times 10^{+02}$	5.7	0.00	0.04	0.07	0.05
990.49(10)	$6.39 \times 10^{+01}$	4.6	−0.21	0.21	−0.29	0.30
992.77(6)	$2.29 \times 10^{+02}$	5.3	0.18	0.07	−0.03	0.10
998.71(12)	$5.27 \times 10^{+01}$	4.1	0.38	0.23	−0.06	0.35
1002.40(6)	$1.72 \times 10^{+02}$	4.6	−0.87	0.08	0.05	0.11
1016.3(8)	$4.19 \times 10^{+02}$	4.3	−0.21	0.04	−0.08	0.05
1018.04(6)	$4.19 \times 10^{+02}$	4.3	−0.21	0.04	−0.08	0.05
1019.2(5)	$4.19 \times 10^{+02}$	4.3	−0.21	0.04	−0.08	0.05
1030.88(6)	$1.80 \times 10^{+02}$	5.5	0.58	0.09	0.17	0.12
1039.78(6)	$2.21 \times 10^{+02}$	6.4	0.19	0.09	−0.23	0.12
1059.87(7)	$1.20 \times 10^{+02}$	4.9	0.19	0.12	−0.12	0.17
1066.04(6)	$1.47 \times 10^{+02}$	4.7	0.24	0.09	0.05	0.13
1075.76(6)	$1.37 \times 10^{+02}$	4.6	0.11	0.10	−0.03	0.14
1079.90(7)	$1.04 \times 10^{+02}$	4.7	0.60	0.13	−0.27	0.19
1086.44(6)	$2.80 \times 10^{+02}$	5.1	−0.64	0.05	0.09	0.07
1101.07(25)	$9.78 \times 10^{+02}$	7.2	0.25	0.02	−0.11	0.03
1103.35(7)	$1.49 \times 10^{+02}$	4.4	−0.64	0.09	0.44	0.10
1111.67(6)	$3.04 \times 10^{+02}$	5.2	−0.14	0.05	0.02	0.06
1114.99(6)	$4.71 \times 10^{+02}$	5.8	−0.23	0.03	−0.06	0.05
1133.36(7)	$1.60 \times 10^{+02}$	5.0	−0.67	0.09	−0.27	0.12
1135.55(6)	$2.82 \times 10^{+02}$	5.5	−0.65	0.06	0.22	0.07
1142.2(3)	$3.43 \times 10^{+03}$	12.0	0.28	0.01	−0.05	0.01
1145.19(7)	$1.42 \times 10^{+02}$	4.5	0.40	0.09	−0.29	0.13
1155.8(1)	$2.03 \times 10^{+02}$	4.0	−0.07	0.06	0.22	0.09
1178.06(6)	$4.51 \times 10^{+02}$	4.9	−0.01	0.03	−0.04	0.05
1181.97(11)	$4.75 \times 10^{+01}$	3.9	−0.60	0.24	0.11	0.32
1201.19(8)	$7.38 \times 10^{+01}$	4.5	0.04	0.18	0.23	0.25
1209.35(50)	$4.63 \times 10^{+01}$	4.6	−0.14	0.29	−0.62	0.43
1231.03(6)	$2.71 \times 10^{+02}$	4.0	−0.26	0.05	−0.26	0.06
1243.08(6)	$9.38 \times 10^{+01}$	3.2	−0.03	0.12	−0.58	0.15
1246.70(9)	$3.86 \times 10^{+01}$	2.9	−0.12	0.27	−1.50	0.35
1246.7(6)	$3.86 \times 10^{+01}$	2.9	−0.12	0.27	−1.50	0.35
1291.21(6)	$3.05 \times 10^{+02}$	6.5	−0.30	0.06	0.08	0.09
1309.66(14)	$3.48 \times 10^{+01}$	4.0	−0.33	0.33	−0.75	0.47
1320.14(8)	$1.21 \times 10^{+02}$	7.1	0.31	0.19	1.09	0.16
1318.84(14)	$1.21 \times 10^{+02}$	7.1	0.31	0.19	1.09	0.16
1323.3(5)	$8.48 \times 10^{+01}$	9.4	0.03	0.41	0.36	0.34
1322.42(10)	$8.48 \times 10^{+01}$	9.4	0.03	0.41	0.36	0.34
1351.01(5)	$2.38 \times 10^{+03}$	10.5	0.03	0.01	−0.01	0.01
1357.95(15)	$3.79 \times 10^{+01}$	4.4	−0.10	0.29	0.02	0.34
1365.85(37)	$7.49 \times 10^{+01}$	4.3	−0.34	0.13	0.75	0.14
1368.6(9)	$4.46 \times 10^{+01}$	3.5	0.41	0.19	1.90	0.15
1443.02(5)	$3.35 \times 10^{+03}$	11.0	0.03	0.01	−0.11	0.01
1460.62(62)	$3.00 \times 10^{+03}$	12.6	0.02	0.01	−0.01	0.02
1461.70(8)	$3.00 \times 10^{+03}$	12.6	0.02	0.01	−0.01	0.02
1491.17(6)	$5.74 \times 10^{+02}$	6.4	0.34	0.03	−0.03	0.05
1506.68(6)	$2.75 \times 10^{+02}$	6.4	−0.30	0.07	−0.05	0.10
1521.74(6)	$2.21 \times 10^{+02}$	4.8	0.14	0.06	0.08	0.09
1521.64(6)	$2.21 \times 10^{+02}$	4.8	0.14	0.06	0.08	0.09
1540.39(11)	$6.00 \times 10^{+01}$	3.7	0.47	0.18	0.25	0.26
1566.04(15)	$4.28 \times 10^{+01}$	3.5	−0.14	0.24	0.23	0.34
1607.04(21)	$1.62 \times 10^{+02}$	5.0	0.11	0.10	−0.07	0.15
1608.16(8)	$1.62 \times 10^{+02}$	5.0	0.11	0.10	−0.07	0.15

TABLE VIII. (Continued.)

E_γ (keV)	A_0	σ_{A_0}	a_2	σ_{a_2}	a_4	σ_{a_4}
1616.56(12)	$1.33 \times 10^{+02}$	44.9	2.12	0.50	1.54	0.41
1627.37(5)	$2.12 \times 10^{+03}$	11.2	−0.07	0.02	−0.02	0.02
1636.49(6)	$4.87 \times 10^{+02}$	6.2	−0.02	0.04	−0.10	0.05
1687.63(5)	$3.58 \times 10^{+03}$	14.7	−0.22	0.01	−0.06	0.02
1710.2(2)	$2.66 \times 10^{+01}$	3.5	−0.70	0.43	−0.08	0.56
1735.67(7)	$1.47 \times 10^{+02}$	5.3	−0.33	0.11	0.02	0.15
1741.53(5)	$2.01 \times 10^{+03}$	11.5	0.30	0.02	−0.06	0.02
1752.2(2)	$4.16 \times 10^{+01}$	7.1	−1.20	0.78	−0.54	0.81
1754.4(2)	$6.75 \times 10^{+01}$	4.8	0.50	0.20	−0.22	0.34
1765.02(6)	$7.04 \times 10^{+02}$	9.3	−0.01	0.04	0.00	0.05
1767.77(6)	$5.29 \times 10^{+02}$	8.7	−0.04	0.05	−0.10	0.07
1849.17(7)	$1.10 \times 10^{+02}$	3.9	−0.28	0.11	−0.30	0.16
1894.03(6)	$2.44 \times 10^{+02}$	5.6	0.28	0.07	−0.06	0.10
1905.30(3)	$1.17 \times 10^{+03}$	9.2	−0.26	0.02	−0.03	0.03
1926.78(6)	$2.12 \times 10^{+02}$	5.0	0.44	0.07	0.02	0.09
1949.72(6)	$1.18 \times 10^{+03}$	9.3	−0.21	0.02	−0.07	0.03
1995.47(7)	$1.43 \times 10^{+02}$	4.9	0.05	0.10	−0.60	0.14
2048.11(11)	$2.31 \times 10^{+02}$	4.7	−0.40	0.03	−0.16	0.08
2106.24(11)	$3.95 \times 10^{+02}$	6.3	−0.11	0.05	−0.14	0.07
2113.93(11)	$5.80 \times 10^{+02}$	8.3	−0.60	0.04	0.03	0.06
2117.2(2)	$3.90 \times 10^{+02}$	7.6	0.30	0.06	−0.24	0.08
2190.45(10)	$3.01 \times 10^{+03}$	14.7	0.16	0.02	−0.15	0.02

TABLE VIII. (Continued.)

E_γ (keV)	A_0	σ_{A_0}	a_2	σ_{a_2}	a_4	σ_{a_4}
2243.61(11)	$2.04 \times 10^{+02}$	5.2	0.00	0.08	−0.15	0.11
2255.32(11)	$4.01 \times 10^{+02}$	6.5	−0.37	0.05	−0.02	0.07
2270.94(14)	$7.27 \times 10^{+01}$	4.2	0.17	0.17	0.05	0.24
2282.51(10)	$8.76 \times 10^{+02}$	8.8	0.19	0.03	−0.18	0.04
2289.30(12)	$1.18 \times 10^{+02}$	4.8	−0.23	0.12	−0.12	0.17
2300.16(12)	$1.16 \times 10^{+02}$	4.8	−0.05	0.13	−0.15	0.18
2314.83(11)	$2.04 \times 10^{+02}$	5.3	0.05	0.08	−0.18	0.11
2337.34(14)	$5.64 \times 10^{+01}$	3.8	−0.72	0.20	−0.92	0.33
2356.60(16)	$6.92 \times 10^{+01}$	3.9	0.78	0.17	0.50	0.24
2396.81(18)	$3.71 \times 10^{+01}$	3.5	0.27	0.30	−0.87	0.45
2403.94(12)	$1.57 \times 10^{+02}$	4.6	0.35	0.09	0.00	0.13
2466.91(11)	$2.92 \times 10^{+02}$	5.7	0.36	0.06	−0.02	0.09
2479.7(2)	$6.99 \times 10^{+01}$	4.0	0.66	0.17	0.63	0.24
2501.4(2)	$5.05 \times 10^{+01}$	4.2	0.13	0.26	0.48	0.42
2607.05(11)	$1.05 \times 10^{+03}$	9.1	−0.11	0.02	−0.06	0.04
2688.61(10)	$1.05 \times 10^{+03}$	10.5	−0.22	0.03	−0.14	0.04
2743.49(11)	$1.27 \times 10^{+03}$	10.6	−0.12	0.02	−0.04	0.02
2887.72(13)	$8.17 \times 10^{+01}$	4.0	0.41	0.14	0.00	0.22
2945.59(11)	$3.83 \times 10^{+02}$	7.4	0.28	0.06	−0.22	0.08
3094.8(5)	$2.61 \times 10^{+02}$	6.2	0.37	0.07	−0.18	0.11
3110.08(51)	$2.77 \times 10^{+02}$	6.5	−0.18	0.07	−0.10	0.10
3128.78(51)	$1.26 \times 10^{+02}$	5.0	0.21	0.12	−0.40	0.18
3196.13(51)	$2.42 \times 10^{+02}$	6.3	0.41	0.07	0.00	0.08
3241.73(51)	$3.15 \times 10^{+02}$	6.0	−0.30	0.05	−0.15	0.08

[1] M. G. Inghram and J. H. Reynolds, Phys. Rev. **78**, 822 (1950).
[2] M. Redshaw, B. J. Mount, E. G. Myers, and F. T. Avignone III, Phys. Rev. Lett. **102**, 212502 (2009).
[3] C. Brofferio, O. Cremonesi, and S. Dell'Oro, Front. Phys. **7**, 86 (2019).
[4] I. Nutini, D. Q. Adams, C. Alduino *et al.*, J. Low Temp. Phys. **199**, 519 (2020).
[5] S. Andringa, E. Arushanova, S. Asahi, M. Askins, D. J. Auty, A. R. Back, Z. Barnard, N. Barros, E. W. Beier, A. Bialek, S. D. Biller, E. Blucher, R. Bonventre *et al.*, Adv. High Energy Phys. **2016**, 1 (2016).
[6] J. Engel and J. Menéndez, Rep. Prog. Phys. **80**, 046301 (2017).
[7] From ENSDF database as of December 1, 2020. Version available at http://www.nndc.bnl.gov/ensarchivals/.
[8] V. Lopac, Nucl. Phys. A **155**, 513 (1970).
[9] K. Heyde and J. L. Wood, Rev. Mod. Phys. **83**, 1467 (2011).
[10] P. E. Garrett, J. L. Wood, and S. W. Yates, Phys. Scr. **93**, 063001 (2018).
[11] A. Kerek, Nucl. Phys. A **176**, 466 (1971).
[12] C. S. Lee, J. A. Cizewski, D. Barker, R. Tanczyn, G. Kumbartzki, J. Szczepanski, J. W. Gan, H. Dorsett, R. G. Henry, L. P. Farris, and H. Li, Nucl. Phys. A **528**, 381 (1991).
[13] A. Neacsu and M. Horoi, Phys. Rev. C **91**, 024309 (2015).
[14] E. Teruya, N. Yoshinaga, K. Higashiyama, and A. Odahara, Phys. Rev. C **92**, 034320 (2015).
[15] A. E. Stuchbery, J. M. Allmond, M. Danchev, C. Baktash, C. R. Bingham, A. Galindo-Uribarri, D. C. Radford, N. J. Stone, and C.-H. Yu, Phys. Rev. C **96**, 014321 (2017).
[16] H. K. Wang, S. K. Ghorui, Z. Q. Chen, and Z. H. Li, Phys. Rev. C **102**, 054316 (2020).
[17] B. J. Coombes, A. E. Stuchbery, J. M. Allmond, A. Gargano, J. T. H. Dowie, G. Georgiev, M. S. M. Gerathy, T. J. Gray, T. Kibédi, G. J. Lane, B. P. McCormick, A. J. Mitchell, N. J. Spinks, and B. P. E. Tee, EPJ Web Conf. **232**, 04003 (2020).
[18] B. Singh, Nucl. Data Sheets **93**, 33 (2001).
[19] S. Sharma, R. Devi, and S. Khosa, Nucl. Phys. A **988**, 9 (2019).
[20] G. Jakob, N. Benczer-Koller, G. Kumbartzki, J. Holden, T. J. Mertzimekis, K.-H. Speidel, R. Ernst, A. E. Stuchbery, A. Pakou, P. Maier-Komor, A. Macchiavelli, M. McMahan, L. Phair, and I. Y. Lee, Phys. Rev. C **65**, 024316 (2002).
[21] A. E. Stuchbery, J. M. Allmond, A. Galindo-Uribarri, E. Padilla-Rodal, D. C. Radford, N. J. Stone, J. C. Batchelder, J. R. Beene, N. Benczer-Koller, C. R. Bingham, M. E. Howard, G. J. Kumbartzki, J. F. Liang, B. Manning, D. W. Stracener, and C.-H. Yu, Phys. Rev. C **88**, 051304(R) (2013).
[22] B. A. Brown, N. J. Stone, J. R. Stone, I. S. Towner, and M. Hjorth-Jensen, Phys. Rev. C **71**, 044317 (2005).
[23] C. Qi, Phys. Rev. C **94**, 034310 (2016).
[24] D. Bianco, N. Lo Iudice, F. Andreozzi, A. Porrino, and F. Knapp, Phys. Rev. C **86**, 044325 (2012).
[25] Y. Lei, Y. M. Zhao, and A. Arima, Phys. Rev. C **84**, 044301 (2011).
[26] S. A. Berendakov, L. I. Govor, A. M. Demidov, and I. V. Mikhailov, Izv. Akad. Nauk SSSR, Ser. Fiz. **52**, 1028 (1988); Bull. Acad. Sci. USSR, Phys. Ser. **52**, 187 (1988).

[27] S. F. Hicks, J. R. Vanhoy, and S. W. Yates, Phys. Rev. C **78**, 054320 (2008).
[28] A. Kerek, P. Carlé, and J. McDonald, Nucl. Phys. A **198**, 466 (1972).
[29] A. Kerek, P. Carlé, and S. Borg, Nucl. Phys. A **224**, 367 (1974).
[30] U. Stöhlker, A. Blönnigen, W. Lippert, and H. Wollnik, Z. Phys. A **336**, 369 (1990).
[31] A. Wolf, R. Moreh, and O. Shahal, Nucl. Phys. A **227**, 373 (1974).
[32] R. Schwengner, G. Winter, W. Schauer, M. Grinberg, F. Becker, P. von Brentano, J. Eberth, J. Enders, T. von Egidy, R.-D. Herzberg, N. Huxel, L. Käubler, P. von Neumann-Cosel, N. Nicolay, J. Ott, N. Pietralla, H. Prade, S. Raman, J. Reif, A. Richter *et al.*, Nucl. Phys. A **620**, 277 (1997).
[33] C. T. Zhang, P. Bhattacharyya, P. J. Daly, Z. W. Grabowski, R. H. Mayer, M. Sferrazza, R. Broda, B. Fornal, W. Królas, T. Pawlat, D. Bazzacco, S. Lunardi, C. Rossi Alvarez, and G. de Angelis, Nucl. Phys. A **628**, 386 (1998).
[34] J. Barrette, M. Barrette, R. Haroutunian, G. Lamoureux, and S. Monaro, Phys. Rev. C **10**, 1166 (1974).
[35] C. J. Barton, M. A. Caprio, D. Shapira, N. V. Zamfir, D. S. Brenner, R. L. Gill, T. A. Lewis, J. R. Cooper, R. F. Casten, C. W. Beausang, R. Krücken, and J. R. Novak, Phys. Lett. B **551**, 269 (2003).
[36] J. S. Dunham, R. T. Westervelt, R. Avida, and S. S. Hanna, Phys. Rev. C **37**, 2881 (1988).
[37] A. E. Stuchbery, A. Nakamura, A. N. Wilson, P. M. Davidson, H. Watanabe, and A. I. Levon, Phys. Rev. C **76**, 034306 (2007).
[38] J. A. Cookson and W. Darcey, Nucl. Phys. **62**, 326 (1965).
[39] J. Burde, G. Engler, A. Ginsburg, A. A. Jaffe, A. Marinov, and L. Birstein, Nucl. Phys. A **141**, 375 (1970).
[40] H. R. Hiddleston, C. L. Hollas, V. D. Mistry, and P. J. Riley, Phys. Rev. C **3**, 905 (1971).
[41] M. Matoba, M. Hyakutake, J. Niidome, K. Yagi, Y. Aoki, and K. Sato, Phys. Lett. B **45**, 463 (1973).
[42] M. Matoba, M. Hyakutake, K. Yagi, and Y. Aoki, Nucl. Phys. A **237**, 260 (1975).
[43] M. Matoba, M. Hyakutake, K. Yagi, Y. Aoki, and C. Rangacharyulu, Nucl. Phys. A **261**, 223 (1976).
[44] Y. S. Kim and B. L. Cohen, Phys. Rev. **142**, 788 (1966).
[45] R. F. Leonard, W. M. Stewart, and N. Baron, Phys. Rev. **162**, 1125 (1967).
[46] P. E. Garrett, N. Warr, and S. W. Yates, J. Res. Natl. Inst. Stand. Technol. **105**, 141 (2000).
[47] E. Sheldon and D. M. Van Patter, Rev. Mod. Phys. **38**, 143 (1966).
[48] R. W. Harper, T. W. Godfrey, and J. L. Weil, Phys. Rev. C **26**, 1432 (1982).
[49] K. B. Winterbon, Nucl. Phys. A **246**, 293 (1975).
[50] B. Fazekas, T. Belgya, G. Molnár, Á. Veres, R. A. Gatenby, S. W. Yates, and T. Otsuka, Nucl. Phys. A **548**, 249 (1992).
[51] T. Belgya, G. Molnár, and S. W. Yates, Nucl. Phys. A **607**, 43 (1996).
[52] S. F. Hicks, J. C. Boehringer, N. Boukharouba, C. Fransen, S. R. Lesher, J. M. Mueller, J. R. Vanhoy, and S. W. Yates, Phys. Rev. C **86**, 054308 (2012).
[53] B. A. Brown and W. D. M. Rae, Nucl. Data Sheets **120**, 115 (2014).
[54] J. M. Allmond, A. E. Stuchbery, B. A. Brown, J. R. Beene, A. Galindo-Uribarri, C. J. Gross, J. F. Liang, E. Padilla-Rodal, D. C. Radford, R. L. Varner, A. Ayres, J. C. Batchelder, A. Bey, C. R. Bingham, M. E. Howard, K. L. Jones, B. Manning, P. E. Mueller, C. D. Nesaraja, S. D. Pain *et al.*, Phys. Rev. C **90**, 014322 (2014).
[55] J. M. Allmond, A. E. Stuchbery, C. Baktash, A. Gargano, A. Galindo-Uribarri, D. C. Radford, C. R. Bingham, B. A. Brown, L. Coraggio, A. Covello, M. Danchev, C. J. Gross, P. A. Hausladen, N. Itaco, K. Lagergren, E. Padilla-Rodal, J. Pavan, M. A. Riley, N. J. Stone, D. W. Stracener *et al.*, Phys. Rev. Lett. **118**, 092503 (2017).
[56] E. E. Peters, A. E. Stuchbery, A. Chakraborty, B. P. Crider, S. F. Ashley, A. Kumar, M. T. McEllistrem, F. M. Prados-Estévez, and S. W. Yates, Phys. Rev. C **99**, 064321 (2019).
[57] E. Caurier, F. Nowacki, A. Poves, and K. Sieja, Phys. Rev. C **82**, 064304 (2010).
[58] M. Danchev, G. Rainovski, N. Pietralla, A. Gargano, A. Covello, C. Baktash, J. R. Beene, C. R. Bingham, A. Galindo-Uribarri, K. A. Gladnishki, C. J. Gross, V. Y. Ponomarev, D. C. Radford, L. L. Riedinger, M. Scheck, A. E. Stuchbery, J. Wambach, C.-H. Yu, and N. V. Zamfir, Phys. Rev. C **84**, 061306(R) (2011).
[59] Y. Khazov, A. A. Rodionov, S. Sakharov, and B. Singh, Nucl. Data Sheets **104**, 497 (2005).
[60] A. A. Sonzogni, Nucl. Data Sheets **103**, 1 (2004).
[61] A. Bockisch and A. M. Kleinfeld, Nucl. Phys. A **261**, 498 (1976).
[62] A. E. Stuchbery, AIP Conf. Proc. **1625**, 52 (2014).
[63] A. E. Stuchbery, J. Phys.: Conf. Ser. **533**, 012046 (2014).
[64] K. Kumar, Phys. Rev. Lett. **28**, 249 (1972).
[65] D. Cline, Annu. Rev. Nucl. Part. Sci. **36**, 683 (1986).
[66] A. Arima, T. Ohtsuka, F. Iachello, and I. Talmi, Phys. Lett. B **66**, 205 (1977).
[67] G. Rainovski, N. Pietralla, T. Ahn, C. J. Lister, R. V. F. Janssens, M. P. Carpenter, S. Zhu, and C. J. Barton, Phys. Rev. Lett. **96**, 122501 (2006).
[68] J. Srebrny, T. Czosnyka, C. Droste, S. Rohoziński, L. Próchniak, K. Zając, K. Pomorski, D. Cline, C. Wu, A. Bäcklin, L. Hasselgren, R. Diamond, D. Habs, H. Körner, F. Stephens, C. Baktash, and R. Kostecki, Nucl. Phys. A **766**, 25 (2006).
[69] J. Srebrny and D. Cline, Int. J. Mod. Phys. E **20**, 422 (2011).
[70] T. Schmidt, K. L. G. Heyde, A. Blazhev, and J. Jolie, Phys. Rev. C **96**, 014302 (2017).
[71] A. Poves, F. Nowacki, and Y. Alhassid, Phys. Rev. C **101**, 054307 (2020).
[72] J. Henderson, Phys. Rev. C **102**, 054306 (2020).